

---

# DORY: OVERCOMING BARRIERS TO COMPUTING PERSISTENT HOMOLOGY

---

A PREPRINT

**Manu Aggarwal\***

manu.aggarwal@nih.gov  
Laboratory of Biological Modeling, NIDDK  
National Institutes of Health  
31 Center Dr, Bethesda, MD 20892

**Vipul Periwal**

vipulp@nidk.nih.gov  
Laboratory of Biological Modeling, NIDDK  
National Institutes of Health  
31 Center Dr, Bethesda, MD 20892

October 20, 2021

## ABSTRACT

Persistent homology (PH) is an approach to topological data analysis (TDA) that computes multi-scale topologically invariant properties of high-dimensional data that are robust to noise. While PH has revealed useful patterns across various applications, computational requirements have limited applications to small data sets of a few thousand points. We present Dory, an efficient and scalable algorithm that can compute the persistent homology of large data sets. Dory uses significantly less memory than published algorithms and also provides significant reductions in the computation time compared to most algorithms. It scales to process data sets with millions of points. As an application, we compute the PH of the human genome at high resolution as revealed by a genome-wide Hi-C data set. Results show that the topology of the human genome changes significantly upon treatment with auxin, a molecule that degrades cohesin, corroborating the hypothesis that cohesin plays a crucial role in loop formation in DNA.

## 1 Introduction

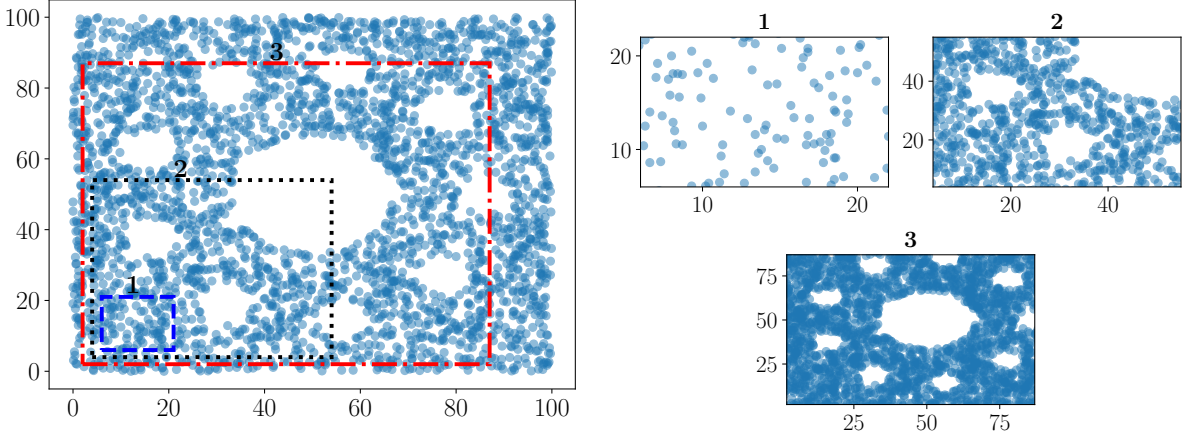
The ever increasing availability of scientific data necessitates development of mathematical algorithms and computational tools that yield testable predictions or give mechanistic insights into model systems underlying the data. The utility of these algorithms is determined by the validity of their theoretical foundations, the generality of their applications, their ability to deal with noisy, high-dimensional, and incomplete data, and the computational scalability. Persistent homology (PH), a mathematically rigorous approach to topological data analysis (TDA), finds patterns in high-dimensional data that are robust to noise, providing a multi-scale overview of the topology of the data.

For example, consider a point-cloud data set of 3000 points (figure 1a). The three rectangles (figure 1b) show different scales of observation of the data. At the small spacial scale (rectangle 1), we do not see a discernible pattern, at a larger scale (rectangle 2), two holes with a distinct pattern appear, and increasing the scale further reveals a third distinct pattern, i.e., the large hole at the center (rectangle 3). For this data set, PH will compute that there are three groups of topologically distinct features. It will also indicate the scale at which they emerge. However, this analysis comes at a high computational cost that has limited the applicability of PH to very small data sets. To introduce these extant

---

\*Corresponding author

computational limitations, we briefly introduce some terminology. A general and detailed exposition on persistent homology can be found in Edelsbrunner and Harer [2008].



(a) A data set with 3000 points. We zoom in at three different scales—rectangle 1, 2, and 3.

(b) New patterns emerge at different scales.

To formalize the notion of topology of a discrete data set, a collection of so-called simplices is defined from the data set as follows: An  $n$ -simplex is a set of  $n + 1$  points and is said to have dimension  $n$  ( $\dim-n$ ). Figure 2a shows different ways to interpret a simplex—as a mathematical set, graphical object, or geometric object—in different dimensions. The *boundary* of an  $n$ -simplex  $\sigma$ , denoted  $\partial\sigma$ , is the set of all  $(n - 1)$ -simplices contained in the simplex. The *coboundary* of an  $n$ -simplex  $\sigma$ , denoted by  $\delta\sigma$ , is the set of all  $(n + 1)$ -simplices  $\omega$  such that  $\sigma \in \partial\omega$ . A collection of simplices is called a *complex*. Figure 2b shows examples of coboundaries and complexes. Contraction can be visualized as a continuous deformation of a simplex to a point. Non-contractible topological structures correspond to obstructions to such a contraction, suggesting the possible existence of a feature in the data.

A hole in  $\dim-d$  is a complex that has a non-contractible boundary in  $\dim-(d - 1)$ . The complex  $D'$  in Figure 2b contains the simplex  $\{a, b, c\}$ , and hence its boundary  $\partial\{a, b, c\} = \{\{a, b\}, \{b, c\}, \{c, a\}\}$  will contract in  $\dim-1$ . On the other hand, since the complex  $D$  does not contain  $\{a, b, c\}$ , its boundary  $\partial\{a, b, c\}$  cannot contract in  $\dim-1$ . Hence,  $D$  contains a non-contractible structure or a hole. These non-contractible structures in  $\dim-d$  define the *homology group* for  $\dim-d$ , denoted by  $H_d$ , partitioned into equivalence classes that are related by contractible simplices. For example, the homology group  $H_1$  of the complex  $D$  has one equivalence class. The non-contractible structures in  $H_0$  can be mapped to path-connected components when the complex is viewed as a discrete graph. Those in  $H_1$  can be mapped to holes on the surface of the triangulation of the point cloud, but are more commonly referred as *loops*, indicative of one dimensional boundaries around the holes. In  $H_2$  they can be thought of as *voids* in an embedding of the triangulation in a three-dimensional metric space, and sets of triangular faces will define their boundaries.

To give a multi-scale overview, PH tracks changes in the homology groups as the scale of observation changes. We see that the collection of simplices in the data set, otherwise known as the complex of the data set, changes at different spacial scales as its construction is based on pairwise distances in the discrete data set. The example (figure 3) shows 4 points in a metric space, with the numbers between two points representing the spacial pairwise distances ( $d(x, y)$ ). At any given scale of observation  $\tau$  we build a complex with all of the 1-simplices  $\{a, b\}$  such that  $d(x, y) \leq \tau$ . Additionally, to compute  $H_d$ , all  $(d + 1)$ -simplices whose boundary is in the complex are also added to it. *This results in a factorial increase in the number of simplices to consider in the complex scaling as the number of points in the data set is raised to a power two larger than the dimension of the homology group.* In figure 3, when  $\tau = 0$ , there are 4 points or 0-simplices. These are indexed arbitrarily from  $\sigma_0$  to  $\sigma_3$ . Starting from  $D_0 = \{\sigma_0\}$ , we define a sequence of complexes  $D_0 \subset D_1 \subset \dots \subset D_n$  such that  $D_i = D_{i-1} \cup \{\sigma_i\}$ . At  $\tau = 0$ , we have  $D_3 = \{\sigma_0, \sigma_1, \sigma_2, \sigma_3\}$ . As  $\tau$  increases, more simplices are added to the complex, and the sequence  $(D_0, \dots, D_{11})$  can be computed for this example. Simplices that are added to the complex at the same value of  $\tau$  can be ordered arbitrarily relative to each other. This sequence of complexes is called the *Vietoris-Rips filtration*.

For every complex in the VR-filtration, we compute the homology groups and record changes in them as we process complexes in the filtration. For example, there is birth of a hole (equivalently, a loop) in  $H_1$  when  $\sigma_8$  is added, which contracts or dies when  $\sigma_{11}$  is added. Birth-death pairs are called persistence pairs, and they are plotted as a function of the scale,  $\tau$ . In our example, the persistence pair is  $(\sigma_8, \sigma_{11})$  in  $H_1$ . These pairs give us *persistence diagrams* (PD), one for every  $H_d$  that is computed. The persistence diagram corresponding to  $H_1$  for this example will contain exactly

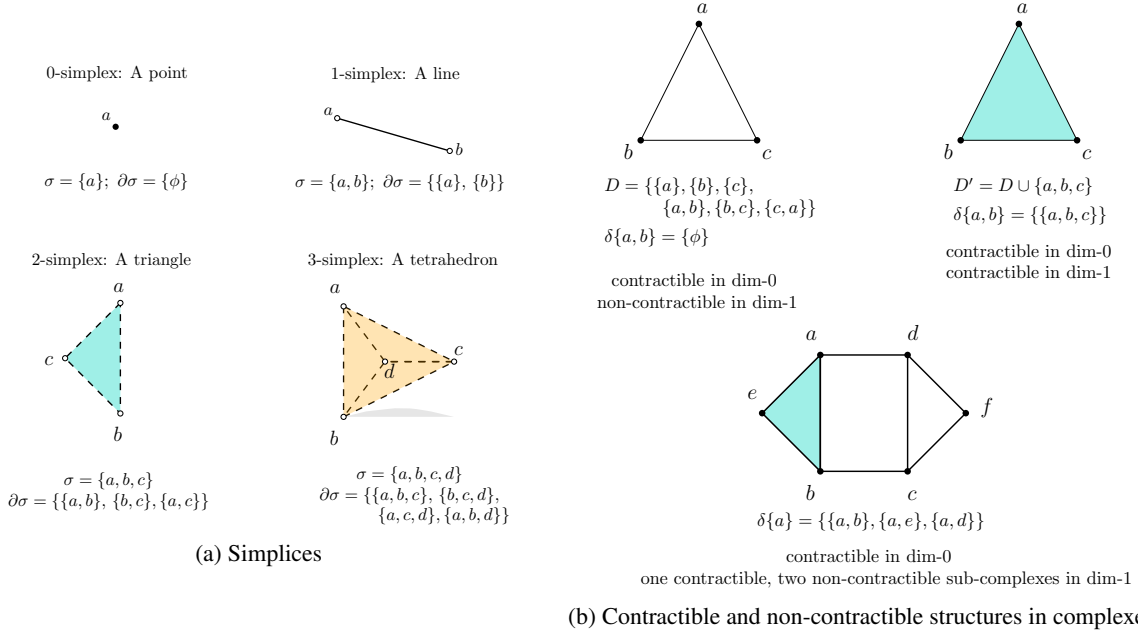


Figure 2: Simplicies form the building blocks for defining a topological space on discrete data set, simplicial topology.

(2.5, 2.75), since  $\sigma_8$  is added at  $\tau = 2.5$  and  $\sigma_{11}$  is added at  $\tau = 2.75$ . The persistence diagram for the example in figure 1a is shown in figure 4b.

It has been shown that the same persistence diagram can be obtained by computing cohomology groups, denoted by  $H_d^*$ . If  $(\sigma, \tau)$  is a persistence pair in  $H_d$ , then  $(\tau, \sigma)$  is a persistence pair in  $H_d^*$ , and consequently,  $|H_d| = |H_d^*|$ . Moreover, the algorithms that compute the persistence pairs of  $H_d$  can also be used to compute the persistence pairs of  $H_d^*$  by applying them to the coboundaries of the complexes in the filtration [De Silva et al., 2011].

As discussed above, computing  $H_2$  across all scales of a data set requires storing and processing all 3-simplices, i.e.,  $O(n^4)$  simplices. Even for a small data set with  $n = 500$  data points, the number of 3-simplices is  $\binom{500}{4} = 2573031125$ , indicative of the memory required to represent the filtration in the computer. Different methods have been developed for storing this information. We compare our algorithm with three software packages—Gudhi, Ripser, and Eirene. Gudhi represents the filtration using a simplex tree [Boissonnat and Maria, 2014], and Ripser [Bauer, 2019] represents a simplex using combinatorial indexing. For large data sets, creating a simplex tree for the entire filtration a priori can require memory up to  $O(n^4)$ , and indexing simplices using combinatorial indexing overflows the bounds of integer data types in most computer architectures. Therefore, both these methods cannot process data sets with large numbers of points. Eirene uses matroid theory that takes more memory than Ripser and, in some cases, more memory than Gudhi. All packages failed to compute PH for at least one data set in our experiments. None were able to process the data set of interest to us, the conformations of the human genome, because of such practical limitations. As PH computation requires processing a combinatorially large number of simplices as well, any method for reducing memory requirements had better not be accompanied by an inordinate increase in computation time either.

Due to these computational difficulties, published algorithms have been practically limited to computing topological features up to and including  $H_2$ . This still allows for applications of PH to a large class of data sets in the physical sciences or to low-dimensional embeddings of high-dimensional data. Therefore, we focus on computing topological features only up to and including the first three dimensions. We take advantage of this restriction to devise a new way to store information and new algorithms to process it, resulting in a reduction in memory requirements by orders of magnitude accompanied with reduced computation time in almost all our test cases.

The two meter long human DNA fits into a nucleus with an average diameter of  $10 \mu\text{m}$  by folding into a complex, facilitated by many proteins which play functional and structural roles [Rowley and Corces, 2018]. This folding is believed to have functional significance so determining topological features like loops and voids in the folded DNA is of interest. Hi-C experiments estimate pairwise spacial distances between genomic loci at 1 kilobase resolution genome [Lieberman-Aiden et al., 2009]. The resulting data set of around 3 million points is analyzed by our algorithm in approximately ten minutes.

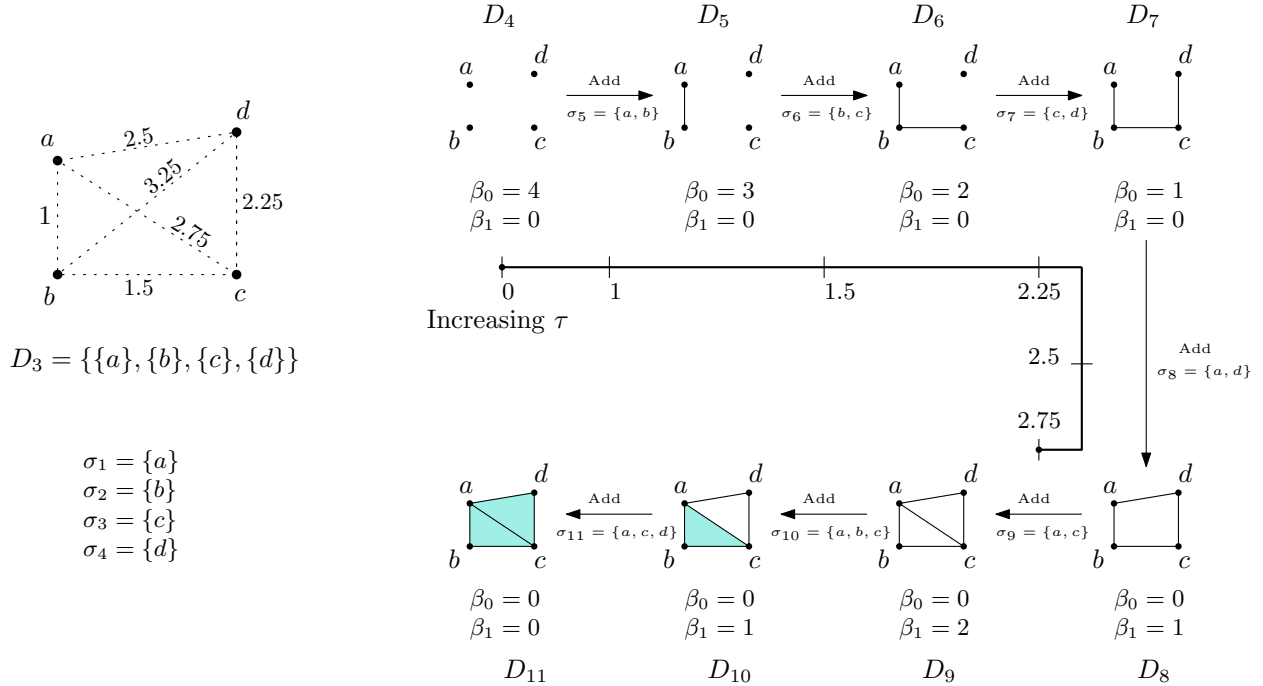


Figure 3: Topological features—number of components ( $\beta_0$ ) and holes ( $\beta_1$ )—change as the scale of observation ( $\tau$ ) changes.

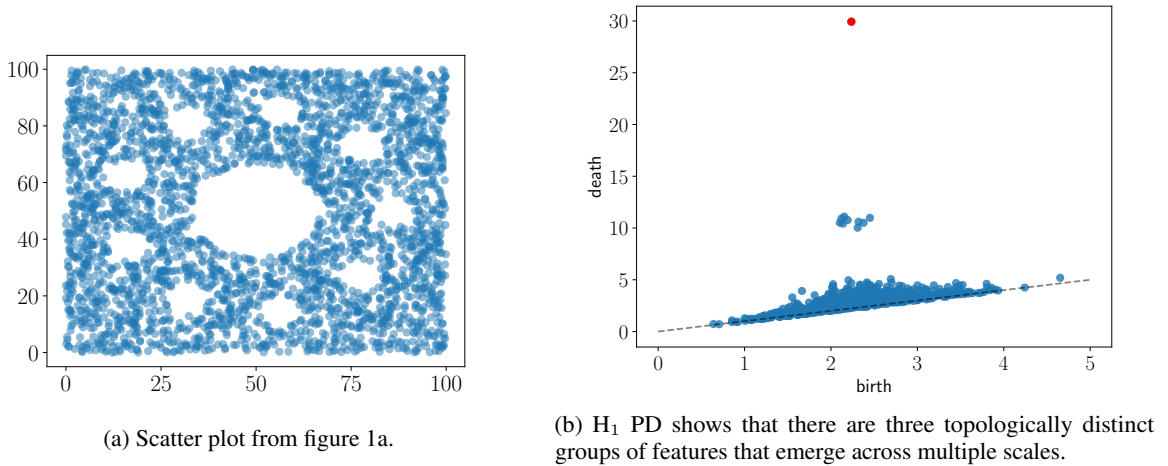


Figure 4: Scatter plot of the data set and its  $H_1$  persistence diagram.

Cohesin is a ring-shaped protein complex that has been shown to colocalize on chromatin along with a highly expressed protein, CTCF, at anchors of loops in the folded chromosome [Rao et al., 2014], indicative of its importance for loop formation in DNA. The  $H_1$  PD corroborates the result of Rao et al. [2017]—cohesin is crucial for loop formation in DNA because, upon addition of auxin, an agent that is known to impair cohesin, the elimination of loops is observed. Additionally, the  $H_2$  PD reveals that auxin treatment leads to a significant reduction in the number of voids.

The rest of this paper is structured as follows: Section 2 introduces the algorithms that form the foundations of Dory. We summarize our contributions in section 3. The algorithm for Dory is explained in section 4. It is then tested with pre-established data sets, and computation time and memory taken are compared with published algorithms in section 5. The analysis of human genome conformations using Hi-C data is in section 6. We end with a discussion in section 7.

## 2 Algorithmic background

An algorithm to compute the persistence birth-death pairs was given by Edelsbrunner et al. [2000], then reformulated as a matrix reduction in Cohen-Steiner et al. [2006]. Any given filtration, viewed as a set of sequences of simplices  $(\sigma_i)_{1 \leq i \leq N}$ , can be represented as a *boundary matrix*  $D = (d_{ij}) \in \mathbb{R}^{N \times N}$ , where  $d_{ij} = 1$  if  $\sigma_i$  is a boundary element of  $\sigma_j$ , and is otherwise 0. Consequently, the indices of the columns and rows of  $D$  represent the simplices indexed according to their order in the filtration. We begin by defining a matrix  $R = D$ . Then,  $\text{low}(j)$  is defined as the largest row index of the non-zero element in column  $j$  of  $R$ , i.e.,  $\text{low}(j) = \arg\max_i \{d_{ij} = 1\}$ . The matrix reduction of  $R$  is formalized as adding (modulo 2) column  $j$  with column  $i$ , for  $i < j$ , until  $\text{low}(j)$  is a *pivot* entry—the first non-zero entry in the row with index  $\text{low}(j)$  is at column  $j$ . This can be written as a matrix multiplication  $DV = R$  (see figure 5a), where  $V$  is the matrix that stores reduction operations and  $R$  is the resulting matrix with all of its columns reduced. In this work we specifically consider addition (modulo 2) of columns for applications to spacial point-cloud data sets. This reduction can be carried out in two ways—standard column algorithm (appendix A, algorithm 6) and standard row algorithm (appendix A, algorithm 7). When all columns of  $R$  have been reduced, the persistence pairs are given by  $(\sigma_{\text{low}(j)}, \sigma_j)$  (born when  $\sigma_{\text{low}(j)}$  is added and died when  $\sigma_j$  is added). Further, if column  $j$  was reduced to  $\mathbf{0}$  but  $j$  is not a pivot of any column of  $R$ , then there is a non-contractible structure in the final complex that was born when  $\sigma_j$  was added to the filtration but it never contracted or died. We represent such a pair by  $(\sigma_j, \infty)$ .

The same  $V$  and, consequently, the same  $R$  are obtained for the standard column and row algorithms [De Silva et al., 2011]. Moreover, reduction of the coboundaries yields the persistence pairs for the cohomology groups,  $H_d^*$ , that are in one-to-one correspondence with the persistence pairs of  $H_d$ . The coboundary matrix is denoted by  $D^\perp = (d_{ij}) \in \mathbb{R}^{N \times N}$ , where  $d_{ij} = 1$  if  $\sigma_{N-i+1}$  is in the coboundary of  $\sigma_{N-j+1}$ , and is otherwise 0. In other words, the columns of  $D^\perp$  are coboundaries, and the indices of the columns and rows of  $D^\perp$  are simplices ordered in the reverse order of the filtration sequence. The matrix setup is shown in figure 5b. De Silva et al. [2011] observed empirically that computing cohomology via the row algorithm provides improvements over homology computation in both time taken and memory requirement.

Figure 5 indicates the size of the matrices when computing PH up to and including the first three dimensions for VR-filtration of a data set with  $n$  points. If  $\tau = \infty$ , the filtration will admit  $\binom{n}{0} + \binom{n}{1} + \binom{n}{2} + \binom{n}{3} + \binom{n}{4} \approx O(n^4)$  simplices (all of the possible 0-, 1-, 2-, and 3-simplices). For a data set with as few as 500 points, the memory requirement just to store  $D$  in a sparse format (storing only the indices of the non-zero elements), is more than 41 GB (presuming 4 bytes per unsigned int).

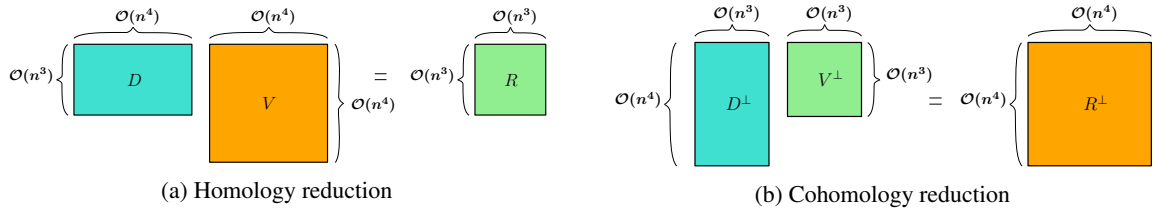


Figure 5: Matrix representation and bounds of PH computation for a data set with  $n$  points.

## 3 Our contribution

- A new way to index 2- and 3-simplices that significantly reduces memory requirement.
- Algorithms to compute coboundaries for edges and triangles using our indexing method that optimize computation time of coboundary traversal during reduction.
- Implicit row reduction algorithm to compute PH that can potentially reduce memory usage by a factor of the number of points in the data set.
- Serial-parallel algorithm that distributes computation of PH over multiple threads without a significant increase in the total memory requirement.
- Two versions of code—sparse and non-sparse. The sparse version requires memory proportional to the number of permissible edges in the filtration. The non-sparse version, while faster, requires memory proportional to the number of total edges possible in the data set.
- Computation of PH of the human genome at high resolution.

## 4 Our algorithm

The aim is to compute persistence pairs up to three dimensions for VR-filtration. We will refer to the 0-simplices as vertices ( $v$ ), 1-simplices as edges ( $e$ ), 2-simplices as triangles ( $t$ ), and 3-simplices as tetrahedrons ( $h$ ). Consider a point-cloud data set embedded in a metric space, i.e., there is a well-defined distance metric between any two points (vertices) in the space. We denote the number of vertices by  $n$ . The number of edges in the filtration, denoted by  $n_e$ , will depend upon the maximum permissible value of the filtration parameter, denoted by  $\tau_m$ . If  $\tau_m$  is small compared to the maximum distance in the data set, we expect  $n_e \ll \binom{n}{2}$  and we call the filtration *sparse*. Since the reduction operations are always between complexes of the same dimension, we construct VR-filtrations for each dimension separately. Let  $\mathcal{S}^d$  be the set of all permissible simplices of dimension  $d$  and  $\mathcal{O}^d$  be the corresponding set of orders in the filtration; we define bijective maps  $f_d : \mathcal{S}^d \rightarrow \mathcal{O}^d$ . Since all vertices are born at the same filtration parameter (zero),  $f_0(v)$  for a vertex  $v$  can be arbitrarily assigned a unique whole number. For convenience, we will use  $f_0(v)$  and  $v$  interchangeably. For edges, the map  $f_1(e)$  is the indexing defined by the sorting algorithm applied to the lengths of the edges. The filtration for 0-simplices is then the list of vertices ordered according to  $f_0$ , and is denoted by  $F_0$ . The filtration for 1-simplices is a list of edges ordered according to  $f_1$ , and is denoted by  $F_1$ . Additionally, we will denote the list of  $d$ -simplices in the reverse order of filtration by  $F_d^{-1}$ . To define filtrations for 2- and 3-simplices we introduce a new way to index triangles and tetrahedrons.

### 4.1 Paired-indexing and neighborhoods

We first define the *diameter* of a simplex  $\sigma$  in the filtration as the maximum of the orders of the edges in the simplex, denoted by  $d(\sigma)$ . The corresponding edge is denoted by  $d^{-1}(\sigma)$ . Then, *paired-indexing* uses a pair of keys, primary ( $k^p$ ) and secondary ( $k^s$ ), denoted by  $\langle k^p, k^s \rangle$ . The primary key for both triangles and tetrahedrons is their diameter and the secondary key is the order of the simplex defined by the remaining points. For a triangle  $t = \{a, b, c\}$ , if  $d^{-1}(t) = \{a, b\}$ , then  $f_2(\{a, b, c\}) = \langle f_1(\{a, b\}), f_0(\{c\}) \rangle = \langle f_1(\{a, b\}), c \rangle$ . For a tetrahedron  $h = \{a, b, c, d\}$ , if  $d^{-1}(h) = \{a, b\}$ , then,  $f_3(\{a, b, c, d\}) = \langle f_1(\{a, b\}), f_1(\{c, d\}) \rangle$ . We define an ordering on the paired-indexing as follows,

$$\langle k_i^p, k_i^s \rangle > \langle k_j^p, k_j^s \rangle \text{ iff either } \{k_i^p > k_j^p\} \text{ or } \{k_i^p = k_j^p \text{ and } k_i^s > k_j^s\}. \quad (1)$$

This ordering on the paired-indexing preserves the order of the simplices in the VR-filtration since a simplex with the larger diameter will have a greater order in the filtration; and simplices with the same diameter can be ordered arbitrarily with respect to each other, which in paired-indexing is based on the secondary key. The maps  $f_2$  and  $f_3$  then define filtrations  $F_2$  and  $F_3$ , respectively. We do not store these filtrations as lists in the algorithm and instead compute them on the fly, reducing the memory required. We say that a simplex in  $\mathcal{S}^d$  is greater than another simplex in  $\mathcal{S}^d$  iff its order in the filtration is greater.

The paired-indexing plays an important role in both reducing memory requirements and computation time. Using the 4 byte `unsigned int`, this indexing will take exactly 8 bytes to represent any triangle or tetrahedron in a filtration regardless of the number of points in the data set. Further, since  $k^p$  and  $k^s$  are less than  $n_e$ , the paired-indices are bounded by  $\mathcal{O}(n_e)$ , rather than  $\mathcal{O}(n^4)$ . This specifically reduces memory requirement by many orders of magnitude for sparse filtrations, where  $n_e \ll \binom{n}{2}$ .

### 4.2 Computing coboundaries

We show how paired-indexing can be used to compute coboundary of edges and triangles. We begin by defining *vertex-neighborhood* ( $N^a$ ) and *edge-neighborhood* ( $E^a$ ) of a vertex  $a$ . Neighbor of the vertex  $a$  is a vertex that shares an edge with  $a$ . Both  $N^a$  and  $E^a$  are lists of all neighbors of  $a$ . Each element of these lists is a structure that contains a neighbor of  $a$  and the order of the edge between them. The vertex-neighborhood is sorted by the order of the neighbors and the edge-neighborhood is sorted by the order of the corresponding edges (see figure 6). The vertex and edge neighborhoods of all vertices are computed using  $F_0$  and  $F_1$ , and they are stored in the memory. We will use  $F_0$  and  $F_1$  in figure 6 as an example to illustrate how paired-indexing can be used to compute coboundary of an edge and a triangle. For convenience, the order of an edge  $\{a, b\}$ ,  $f_1(\{a, b\})$ , is denoted by  $ab$ .

#### 4.2.1 Coboundaries of edges

Consider the edge  $\{a, b\}$  in figure 6. Any simplex in its coboundary is a triangle  $t = \{a, b, v\} = \langle k_1, k_2 \rangle$ , where  $v$  is a common neighbor of  $a$  and  $b$ ; and the diameter of  $t = k_1 \geq ab$ . We consider two cases: case 1, triangles with diameter equal to  $ab$ , and case 2, triangles with diameter greater than  $ab$ . The triangles in case 1 are smaller than those in case 2.

$F_0$	a	b	c	d	e	f	g	h						
$F_1$	de	ah	bh	ae	be	eh	ac	bf	ab	ad	bg	af	bd	ef

$N^a$	neighbor	b	c	d	e	f	h
	$f_1(\text{edge})$	ab	ac	ad	ae	af	ah

$E^a$	neighbor	h	e	c	b	d	f
	$f_1(\text{edge})$	ah	ae	ac	ab	ad	af
		0	1	2	3	4	5

Figure 6: An example of a VR-filtration.  $F_0$  is the list of vertices and  $F_1$  is the list of edges, both sorted in the order of the filtration. The vertex- and edge-neighborhoods for vertex  $a$  are shown as example. The dark border indicates that  $N^a$  is sorted by the order of neighbors of  $a$  and  $E^a$  is sorted by the order of the corresponding edges.

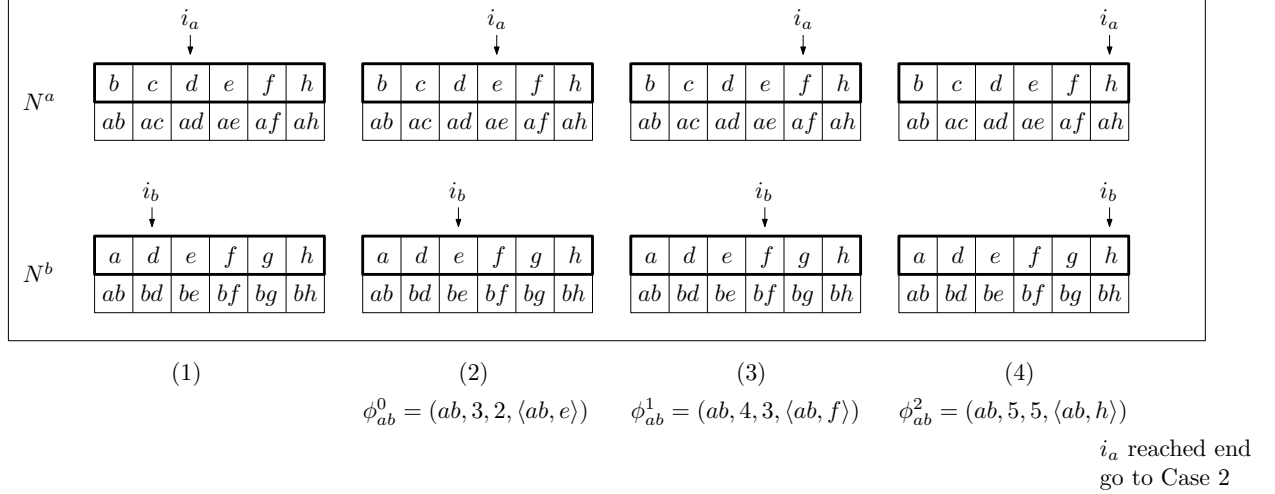
Hence, to compute the simplices in the coboundary as ordered in  $F_2$ , we start in case 1—the primary key is  $ab$  and the order of the simplices is decided by the vertex in  $t$  that is not  $a$  and  $b$ , i.e.,  $v$ . We traverse along the vertex-neighborhoods using indices  $i_a$  and  $i_b$  to find common neighbors in an increasing order. Initially, both are set to 0. As shown in figure 7, we increment the index pointing to the lower ordered vertex till both indices point to the same vertex  $v$ ; in which case,  $v$  is a common neighbor and  $\{a, b, v\}$  exists in the filtration. However, we have to ensure that its diameter is  $ab$  since we are in case 1. For example, in (1) in figure 7, we skip  $\{a, b, d\}$  because  $ad > ab$  (see  $F_1$  in figure 6). Note that the structures in vertex-neighborhoods give direct access to  $av$  and  $bv$  at  $i_a$  and  $i_b$  for comparison with  $ab$ . Otherwise, if the diameter of  $\{a, b, v\} = ab$ , then  $\langle ab, v \rangle$  is the next greater triangle in  $\delta\{a, b\}$  in  $F_2$ . This triangle is recorded as  $\phi = (ab, i_a, i_b, \delta_*)$  where  $\delta_* = f_2(\{a, b, v\}) = \langle ab, v \rangle$ . We call this the  $\phi$ -representation of  $\delta_*$  as a simplex in the coboundary of  $\{a, b\}$ . If either of the indices reach the end of the corresponding neighborhood, we go to case 2.

In case 2, the triangles in  $\delta\{a, b\}$  have diameter greater than  $ab$ . Hence, their order in the filtration is defined by the diameter of the primary key. To compute the primary keys as ordered in  $F_2$ , we define  $i_a$  and  $i_b$  to be indices of the respective edge-neighborhoods since they are sorted by the order of the edges. We set  $i_a$  and  $i_b$  to point to the smallest edges greater than  $ab$  (binary search operations in  $E^a$  and  $E^b$ , respectively). We then consider the index that points to the lower ordered edge. For example, in (7) in figure 7,  $i_a = 3$  points to  $ad$  and  $i_b = 3$  points to  $bg$ . We consider  $i_a = 3$  because  $ad < bg$ . Now, we have to check that  $\{a, b, d\}$  exists and its diameter is  $ad$ . A single binary search operation over  $N^b$  finds that  $d$  is a neighbor of  $b$ , confirming the existence of  $\{a, b, d\}$ , and it also gives us  $bd$ . Since  $ad < bd$ , the diameter of  $\{a, b, d\}$  is not  $ad$  and we do not record it as a coboundary. We proceed by incrementing  $i_a$  by one. Now  $i_b$  points to the smaller edge, and the corresponding triangle is  $\{a, b, g\}$ . A binary search over  $N^b$  finds that  $g$  is not a neighbor of  $a$ , hence, this triangle does not exist, and  $i_b$  is incremented by 1 to continue. The index  $i_a$  now points to the smaller edge ( $af$ ), and the corresponding triangle is  $\{a, b, f\}$ . Since, this triangle exists and  $af$  is its diameter,  $\langle af, b \rangle$  is the next simplex in the coboundary and it is recorded as  $\phi = (ab, i_a, i_b, \langle af, b \rangle)$ . This process is continued till both  $i_a$  and  $i_b$  reach the end of the respective edge-neighborhood.

The above computation yields the coboundary of  $\{a, b\}$  as a list of tuples  $\phi_{ab}^i$  (see figure 7) in an increasing order. This is an inefficient method to compute the coboundary of a simplex if it needs to be computed only once. A faster method would be to create the entire list of simplices in the coboundary and sort it by the order. However, reduction can require the computation of the coboundary of a simplex multiple times. Further, it is not feasible to store the entire coboundary matrix a priori due to memory limitations—even the size of the coboundary of one simplex can be up to  $O(n^4)$  (see figure 5). Using our  $\phi$ -representation, we implement three algorithms to address both these issues. First, the smallest simplex in the coboundary of  $\{a, b\}$  can be found simply by starting in case 1 with  $i_a$  and  $i_b$  initialized to 0, and proceed as outlined previously. The first valid simplex encountered is the answer. This is implemented as `FindSmallestt` (algorithm 10). Second, given a tuple  $\phi = (ab, i_a, i_b, \langle k_1, k_2 \rangle)$ , the next greater simplex in  $\delta\{a, b\}$  can be computed as follows. If  $k_1 = ab$ , then  $i_a$  and  $i_b$  are indices of the vertex-neighborhoods (case 1) and if  $k_1 > ab$ , they are indices of edge-neighborhoods (case 2). After determining the scenario, we proceed as outlined previously. As a result, given the  $\phi$ -representation of a triangle  $t$  in the coboundary of an edge  $\{a, b\}$ , we can compute the next greater triangle in its coboundary without always having to traverse entire neighborhoods of  $a$  and  $b$ . We implement this as `FindNextt` (algorithm 11). Third, given a triangle  $\delta_{\#} = \langle k_1, k_2 \rangle$ , the smallest simplex greater than or equal to  $\delta_{\#}$  in the coboundary of an edge  $\{a, b\}$  can be computed by considering three scenarios. (1) If  $k_1 < ab$ , then the triangle with the least order in the coboundary of  $\{a, b\}$  is the answer. (2) If  $k_1 = ab$ , then we start in case 1 at indices  $i_a$  and  $i_b$  of vertex-neighborhoods that point to the neighbor with smallest order greater than or equal to  $k_2$ ; if no such neighbor exists, then we initialize  $i_a$  and  $i_b$  to the beginning of case 2. (3) If  $k_1 > ab$ , then we start in case 2 at the indices  $i_a$  and  $i_b$  of edge-neighborhoods that point to the edges with smallest order greater than or equal to  $k_1$ . This algorithm

reduces the processing time by determining optimal initial values of the indices. This is implemented as FindGEQt (algorithm 12). Note that the search operations in all of these algorithms are binary search operations since vertex- and edge-neighborhoods are sorted. See appendix B for all the pseudocodes related to coboundaries of edges.

Case 1



Case 2

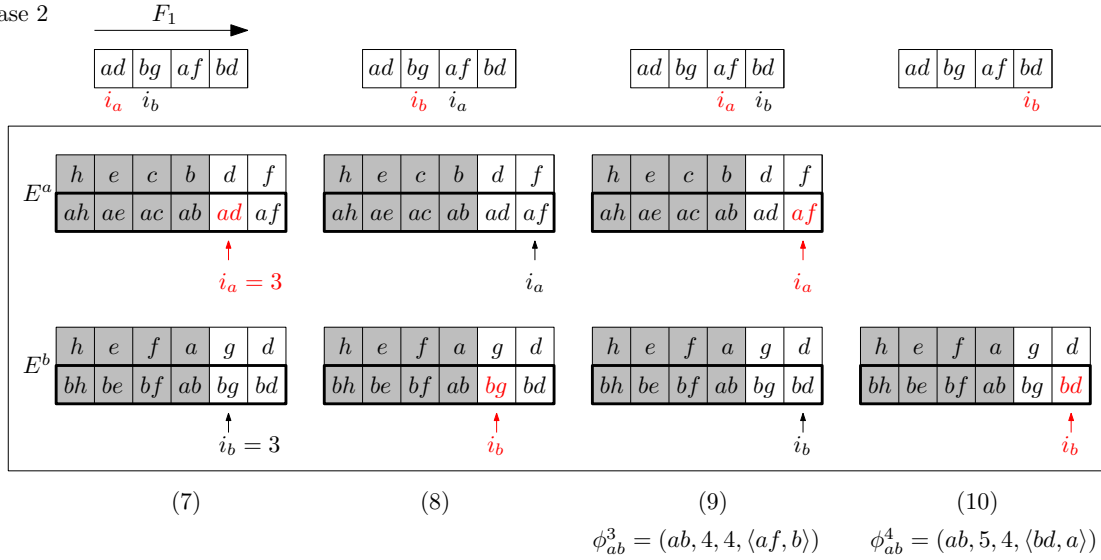


Figure 7: Using vertex- and edge-neighborhoods to compute simplices in the coboundary of edge  $\{a, b\}$  (see figure 6 for  $F_1$ ), such that they are in the order of  $F_2$ . The valid triangles are stored using  $\phi$ -representation.

#### 4.2.2 Coboundaries of triangles

Consider the triangle  $t = \{a, b, e\} = \langle ab, e \rangle$  in figure 6. Any simplex in its coboundary is a tetrahedron  $t = \{a, b, e, v\} = \langle k_1, k_2 \rangle$ , where  $v$  is a common neighbor of  $a, b$ , and  $e$ ; and the diameter of  $h = k_1 \geq ab$ . We will use three indices,  $i_a, i_b$ , and  $i_e$ , to keep track of neighborhoods of  $a, b$ , and  $e$ , respectively. We consider two cases: case 1, tetrahedrons with diameter equal to  $ab$ , and case 2, tetrahedrons with diameter greater than  $ab$ . The tetrahedrons in case 1 are smaller than the triangles in case 2, so we start with case 1—the primary key is  $ab$  and the order of the simplices is decided by the order of the edge  $\{e, v\}$ . To compute such edges according to their order in  $F_1$ , we traverse through the edge-neighborhood of  $e$ . Initially,  $i_e$  is set to 0. For every edge  $\{e, v\}$  that  $i_e$  points to, we check whether  $v$  is a neighbor of  $a$  and  $b$  to confirm existence of  $\{a, b, e, v\}$ , and we check that  $ab$  is its diameter. These checks require two binary search operations, one each for  $N_a$  and  $N_b$ . If both conditions are satisfied, then we record the tetrahedron. We proceed by incrementing  $i_e$  by one. For example, when  $i_e = 0$  in (1) in figure 8, the resulting tetrahedron exists but  $ab$  is not its diameter, and we do not record it. We skip when  $i_e$  points to  $ae$  or  $be$  because they are not valid tetrahedrons. The first



tetrahedron with diameter  $ab$  is when  $i_e = 3$ , and hence,  $\{a, b, e, h\}$  is the smallest tetrahedron in  $\delta t$ . We define the  $\phi$ -representation for tetrahedrons as the tuple  $\phi = (t, i_a, i_b, i_e, f, \langle ab, eh \rangle)$ , where  $f$  flags the diameter as follows—if  $f = 0$ , the diameter is  $ab$ ;  $f = 1$ , it is  $ah$ ;  $f = 2$ , it is  $bh$ ; and  $f = 3$ , diameter is  $eh$ . This flag is implemented to determine which index has to be incremented to find the next greater tetrahedron in  $\delta t$ . For example, if  $ab$  is the diameter, i.e.  $f = 0$ , we are in case 1 and  $i_e$  is to be incremented by one to proceed. Note that, in general, for any given triangle  $t = \langle k^p, k^s \rangle$ , we compute  $a \leftarrow \min\{f_1^{-1}(k^p)\}$ ,  $b \leftarrow \max\{f_1^{-1}(k^p)\}$ , and  $e \leftarrow k^s$ . Case 1 is continued till  $i_e$  points to an edge greater than  $ab$ , since all tetrahedrons henceforth will have a diameter greater than  $ab$ . In figure 6,  $ef > ab$  (indicated by a dashed line), hence we start with case 2 when  $i_e = 3$ .

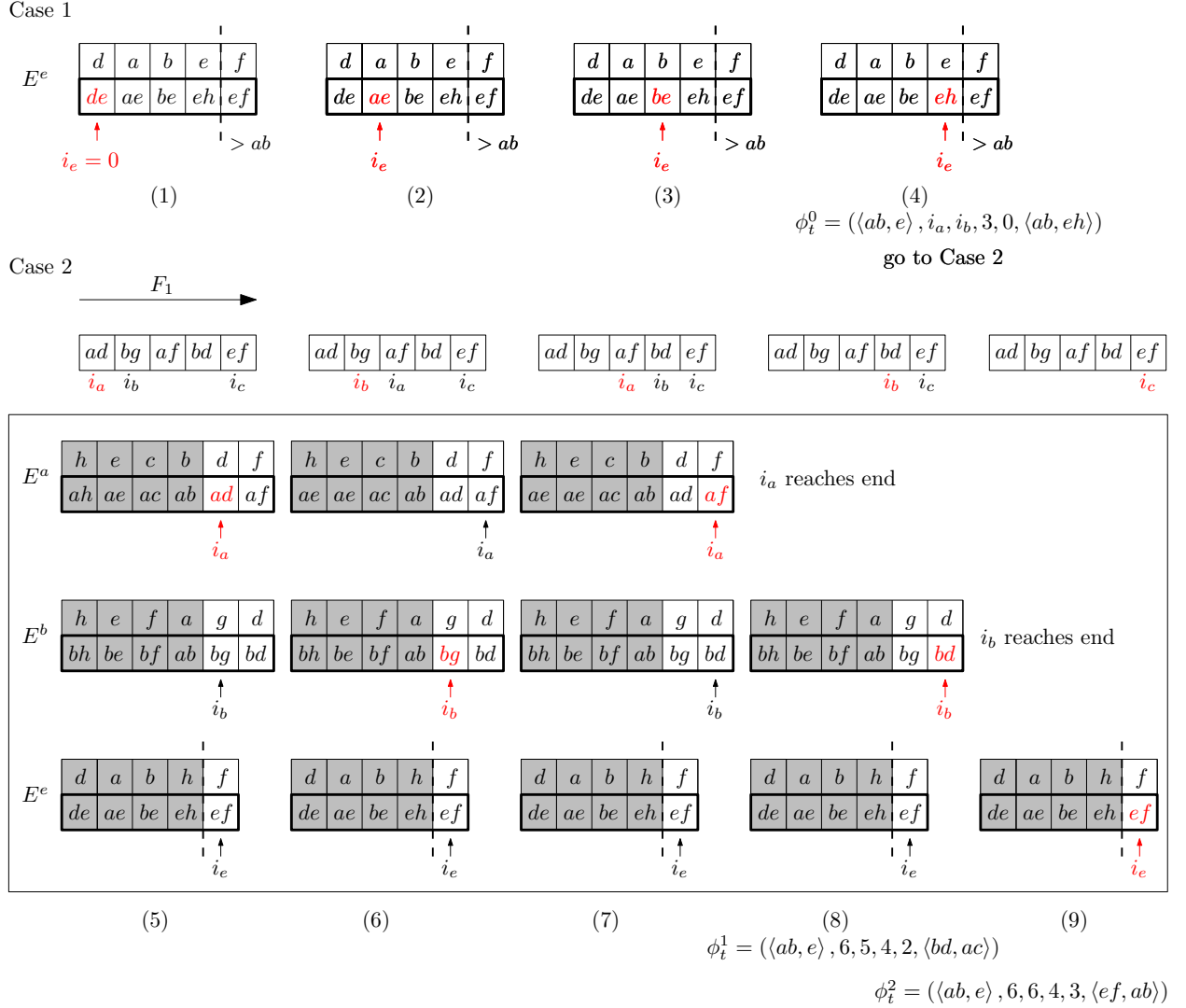
All valid tetrahedrons in case 2 that are in  $\delta t$  will have diameter greater than  $ab$ . The index  $i_e$  already points to the entry in  $E^e$  that has the smallest edge greater than  $ab$ ; and we implement binary search to compute  $i_a$  and  $i_b$  such that they also point to the smallest edge greater than  $ab$  in the respective edge-neighborhood. All tetrahedrons in case 2 will have different primary keys since they have different diameters. Among the indices  $i_a, i_b$ , and  $i_e$ , we consider the index that is pointing to the edge with the minimum order. As before, we have to check the existence of the tetrahedron and that its diameter is the edge under consideration. For example, in figure 8, we begin case 2 in (5) by considering  $i_a$  because it points to  $ad = \min\{ad, bg, ef\}$ . Binary searches for vertex  $d$  over  $N^b$  and  $N^e$  confirm the existence of the tetrahedron  $\{a, b, e, d\}$  and also show that  $ad$  is not its diameter. Hence, this tetrahedron is not recorded and  $i_a$  is incremented by 1 to proceed. Now,  $i_b$  points to the smallest edge, but the resulting tetrahedron does not exist since  $g$  is not a neighbor of  $e$ . The smallest tetrahedron in case 2 is  $\{a, b, e, d\}$ , recorded at (8) as  $(\langle ab, e \rangle, 6, 5, 4, 2, \langle bd, ac \rangle)$ . Note that  $f$  is 2 since the diameter is  $bd$ . This flag dictates that  $i_b$  is to be incremented by 1 to proceed because the current pointer being considered is  $i_b$ . Similarly, if  $f = 1$  then  $ad$  is the diameter and  $i_a$  has to be incremented to proceed and if  $f = 3$ , then  $ed$  is the diameter and  $i_e$  has to be incremented by 1. The index  $i_e$  is incremented to proceed when either  $f = 0$  or  $f = 3$ , but we are in case 1 in the former and in case 2 in the latter. Case 2 ends when all three indices reach the end of their respective edge-neighborhood.

The above computation yields the coboundary of  $t = \{a, b, e\}$  as a list of tuples  $\phi_t^i$  (see figure 8). The case and the index to be incremented is determined by the flag  $f$  as discussed previously. As done for edges, this  $\phi$ -representation is used to implement three algorithms—FindSmallesth, FindNexth, and FindGEQh. The smallest simplex in the coboundary of  $t$  can be found simply by starting in case 1, initializing  $i_e$  to 0, and proceeding as outlined previously. The first valid simplex encountered is the answer (algorithm 15). For FindNexth (algorithm 16), given the  $\phi$ -representation of a simplex  $\langle k_1, k_2 \rangle$  in  $\delta t$  as  $\phi = (t, i_a, i_b, i_e, f, \langle k_1, k_2 \rangle)$ , the smallest simplex greater than  $\langle k_1, k_2 \rangle$  in  $\delta t$  can be computed by proceeding in case 1 if  $f = 0$  and proceeding in case 2 otherwise—incrementing the indices by one as dictated by the value of  $f$ . Finally, given a tetrahedron  $\delta_{\#} = \langle k_1, k_2 \rangle$ , the search for smallest simplex greater than or equal to  $\delta_{\#}$  in  $\delta t$  is optimized by considering three scenarios (algorithm 17). (1) If  $k_1 < ab$ , then the smallest tetrahedron in  $\delta t$  (FindSmallesth) is the answer. (2) If  $k_1 = ab$ , then we start in case 1 and search for  $i_e$  that points to the smallest edge greater than or equal to  $k_2$ . If no such edge exists, then we start at case 2 with  $i_e$  pointing to the end of  $E^e$ . (3) If  $k_1 > ab$ , we are in case 2 and we find the indices that greater than or equal to  $k_1$  in the respective edge-neighborhoods. See appendix C for all the pseudocodes related to coboundaries of triangles.

### 4.3 Cohomology reduction: Memory optimizations

To compute the persistence pairs using cohomology reduction, we reduce one simplex at a time since it is often not feasible to store the coboundary matrix  $D^{\perp}$ . Suppose the reduced coboundaries are stored in  $R^{\perp}$  and the reduction operations are stored in  $V^{\perp}$ . We will denote the column in  $R^{\perp}$  that contains the reduced coboundary of edge  $e$  by  $R^{\perp}(e)$  and the corresponding column in  $V^{\perp}$  by  $V^{\perp}(e)$ . Using this notation, the column reduction to reduce coboundary of one edge at a time is shown in algorithm 1. Here,  $\text{low}(R^{\perp}(e))$  is the simplex with the smallest order in column  $R^{\perp}(e)$ . The partial reduction of the edge is stored in  $r$  which initially is the coboundary of the edge. If  $\text{low}(r) = \text{low}(R^{\perp}(e'))$  for some edge  $e'$ , then  $r$  is reduced (sum modulo 2) with  $R^{\perp}(e')$ . If no such edge exists or if  $r$  is  $\mathbf{0}$ , then  $r$  is completely reduced. A non-empty completely reduced  $r$  is recorded as the column  $R^{\perp}(e)$  or  $R^{\perp}$ , and  $(\text{low}(R^{\perp}(e)), e)$  is a persistence pair.

However, figure 5b shows that  $R^{\perp}$  has the worst bounds on size. Therefore, we store only the reduction operations, i.e.,  $V^{\perp}$ . Then,  $r$  can be implicitly reduced with  $R^{\perp}(e')$  by summing (modulo 2) it with the coboundaries of edges in  $V^{\perp}(e')$  (see algorithm 2). The smallest simplex  $t$  after reducing coboundary of an edge  $e'$  is stored as a persistence pair  $(t, e')$  in  $p^{\perp}$ . In this algorithm, the partial reduction operations are recorded in  $v$ , the result of the ongoing reduction is in  $r$ , and the smallest simplex in  $r$  is stored as  $\delta_*$ . However, keeping track of  $r$  can require a lot of computer memory as its length is bounded by  $O(n^3)$  (and by  $O(n^4)$  when reducing triangles). We developed an implicit row algorithm that does not store  $r$  at any stage of reduction, and implicitly reduces  $r$  using  $v$ . Hence, its memory requirement depends on the size of  $v$ — $O(n^2)$  for reducing edges and  $O(n^3)$  for reducing triangles, potentially reducing the memory requirement by an order of  $n$ .

**Algorithm 1** Starting with standard column reduction

- 1: **Input:**  $F_1$
- 2:  $R^\perp$  is empty
- 3: **for**  $e$  in order of  $F_1^{-1}$  **do**
- 4:    $r \leftarrow \delta e$
- 5:   **while**  $r$  not empty AND there exists edge  $e'$  s.t.  $\text{low}(R^\perp(e')) = \text{low}(r)$  **do**
- 6:      $r \leftarrow r \oplus R^\perp(e')$
- 7:   **if**  $r$  not empty **then**
- 8:      $R^\perp(e) \leftarrow r$

---

**Algorithm 2** Do not store  $R^\perp$ : Implicitly compute from  $V^\perp$ 


---

```

1: Input:  $F_1$ 
2:  $V^\perp, p^\perp$  are empty
3: for  $e$  in  $F_1^{-1}$  do
4:    $r \leftarrow \delta e$ 
5:    $\delta_* \leftarrow \text{low}(r)$ 
6:    $v \leftarrow [e]$ 
7:   while  $\delta_*$  is not empty AND there is a pair  $(\delta_*, e')$  in  $p^\perp$  do
8:     for  $e''$  in  $V^\perp(e')$  do
9:        $r \leftarrow r \oplus \delta e''$ 
10:     $\delta_* \leftarrow \text{low}(r)$  ▷ Update the low
11:     $v \leftarrow v \oplus V^\perp(e')$  ▷ Update reduction operations for  $e$ 
12:   if  $\delta_*$  not empty then
13:      $V^\perp(e) \leftarrow v$ 
14:      $p^\perp \leftarrow (\delta_*, e)$ 

```

---

### 4.3.1 Implicit row algorithm

The reduction of the coboundary of an edge requires the computation of the smallest triangle in  $r$  with non-zero coefficient, denoted by  $\delta_*$  in the algorithm. Implicitly,  $\delta_*$  is the smallest triangle with non-zero coefficient after coboundaries of all edges in the corresponding  $v$  are summed. We will use the  $\phi$ -representation to store information in  $v$ , compute coboundaries using `FindSmallestt`, `FindNextt`, and `FindGEQt`, and compute  $\delta_*$  using row-algorithm. To explain the algorithm, we will walk through an example that reduces  $r = \delta e_0$  with  $R^\perp$  using only  $v$ ,  $V^\perp$ , and  $p^\perp$ .

Step 1 ('initialize' in figure 9): As shown in the figure,  $\delta^0$  is the smallest simplex in  $\delta e_0$ . Then,  $v$  is initialized as a list with the single entry of  $\phi$ -representation of  $\delta^0$  in  $\delta e_0$ , denoted by  $\phi_{e_0} = (e_0, i_a, i_b, \delta^0)$ . This corresponds to the information that  $r = \delta e_0$  initially and the smallest triangle in  $r$  is  $\delta^0$ . Subsequently,  $\delta_*$  is initialized with  $\delta^0$ .

Step 2 ('append' in figure 9): Now, suppose there exists a pair  $(\delta_*, e')$  in  $p^\perp$  and  $V^\perp(e') = [e'_1, e'_2, e'_3]$ . Then,  $r$  is to be summed with  $R^\perp(e')$ . Since the smallest triangle with non-zero coefficient in  $R^\perp(e')$  is  $\delta_*$ , we know that when coboundaries of all  $e'_k$  in  $V^\perp(e')$  are summed with each other, then every triangle that is smaller than  $\delta_*$  will have a zero coefficient (shown as shaded area in the figure). Hence, triangles in  $\delta e'_k$  that are smaller than  $\delta_*$  will have zero coefficient and they do not matter. Therefore, for every edge  $e'_k$  in  $V^\perp(e')$  and the edge  $e'_0$ , we use `FindGEQt` to compute the smallest triangle in their coboundary that is greater than or equal to  $\delta_*$ , and append its  $\phi$ -representation to  $v$  (see (0) in figure 9). The updated  $v$  corresponds to the updated  $r \leftarrow r \oplus R^\perp(e')$ , therefore the coefficient of  $\delta_*$  will be 0. To find the smallest triangle with non-zero coefficient in  $r$ , we go to step 3.

Step 3 ('reduce' in figure 9): We first define  $\delta = \text{MAX} = \langle n_e, 0 \rangle$  (since  $k_1 < n_e$ ), and then process every  $\phi_e = (e, i_a, i_b, \delta_e)$  in  $v$  as follows. If  $\delta_e = \delta_*$ , then we find the next simplex greater than  $\delta_e$  in coboundary of  $e$  using `FindNextt` since the coefficient of  $\delta_*$  is 0. If the updated  $\delta_e$  is less than  $\delta$ , then we set  $\delta \leftarrow \delta_e$  and set the coefficient to 1, otherwise, 1 is added (modulo 2) to the coefficient. As a result,  $\delta$  stores the smallest triangle greater than  $\delta_*$  in  $r$ , and we also keep track of its coefficient. For example, starting at (0) in figure 9,  $\delta_e = \delta_1$  for the edges  $e'_3, e'_2, e'_1$ , and  $e_0$ . For these edges we compute the next greater triangle in their respective coboundary using `FindNextt`. After iterating through all entries in  $v$ , it is determined that  $\delta^1$  is the smallest simplex greater than  $\delta_*$ , and it has a coefficient of 0 (see (1) in figure). We update  $\delta_* \leftarrow \delta^1$ ;  $\delta \leftarrow \text{MAX}$ ; and iterate through all entries in  $v$  as done previously. In (3) we get  $\delta_* = \delta^2$  with non-zero coefficient. This signals the end of implicit reduction of  $r$  with  $R^\perp(e'_0)$ . To determine whether  $r$  is to be reduced with another column of  $R^\perp$ , we check if there exists a persistence pair  $(\delta_*, e'')$  in  $p^\perp$  and go back to step 2 to append  $V^\perp(e'')$  to  $v$ . Otherwise,  $r$  is completely reduced and we go to the next step to update  $p^\perp$  and  $V^\perp$ . In general, it is possible that  $\delta_*$  is empty, in which case  $r$  was reduced to  $\mathbf{0}$  and reduction ends without requiring any update to  $p^\perp$  and  $V^\perp$ .

Step 4 ('update' in figure 9): If  $\delta_*$  is not empty, then we add the persistence pair  $(\delta_*, e_0)$  to  $p^\perp$ . To update  $V^\perp$ , we first sum all  $\phi_e$  modulo 2. This is because a  $\phi_e$  with zero coefficient implies that the entire coboundary of  $e$  will sum to 0 when coboundaries of all edges in  $v$  are summed. For every  $\phi_e$  with non-zero coefficient, except for  $\phi_{e_0}$ , we append  $e$  to the column  $V^\perp(e_0)$ . The edge  $e_0$  is not appended to  $V^\perp(e_0)$  because  $\phi_{e_0}$  will always have a coefficient 1 and we already store  $e_0$  in the persistence pair  $(\delta_*, e_0)$ . If the resulting  $V^\perp(e_0)$  is empty, then we do not make any record of it. This concludes the complete reduction of  $r$  with  $R^\perp$ .

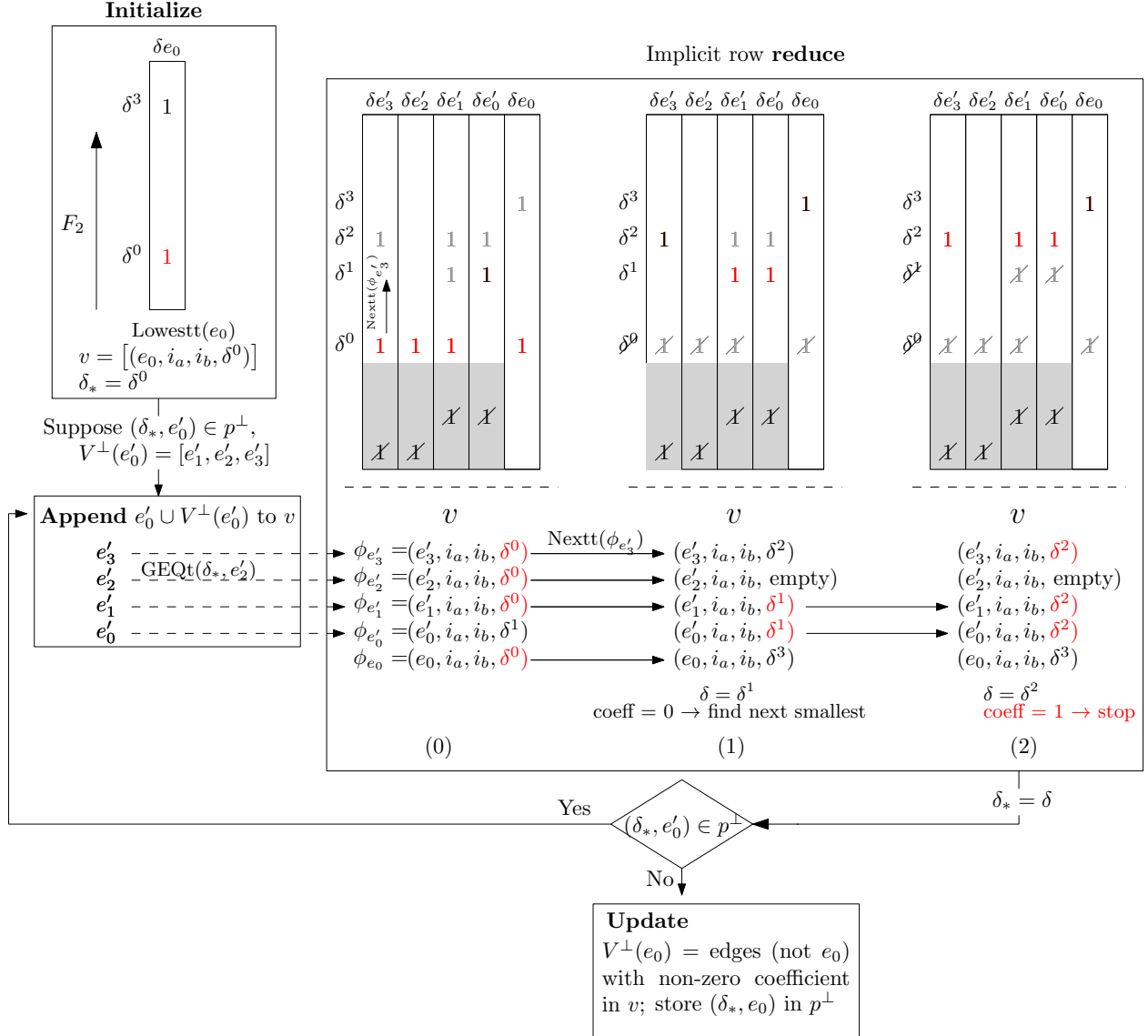


Figure 9: Example to show implicit reduction of  $r = \delta e_0$  with  $R^\perp$  using  $V^\perp$  and  $p^\perp$ . For every edge in  $v$ , we record the smallest triangle in its coboundary with non-zero coefficient using the  $\phi$ -representation (marked in black). The smallest among these are marked in red. Simplices with zero coefficient are shown as crossed out.

The implicit row algorithm to compute  $H_2^*$  similarly reduces the coboundary of a triangle by using the  $\phi$ -representation for tetrahedrons introduced in section 4.2.2 along with the functions `FindSmallesth`, `FindNexth`, and `FindGEQh`.

### 4.3.2 Trivial persistence pairs

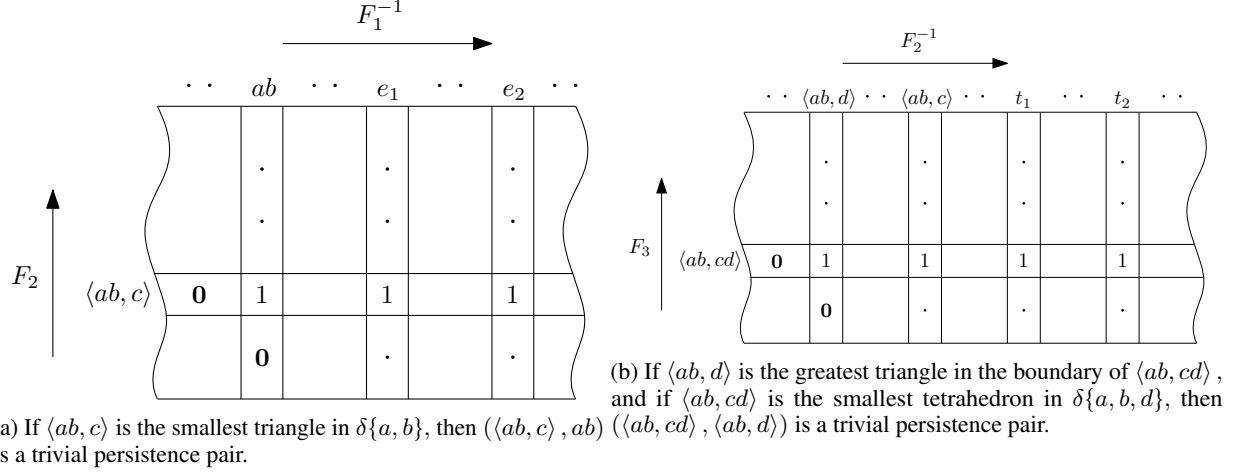


Figure 10: Trivial persistence pairs

For further reduction in memory usage, we notice that there are specific persistence pairs that can be computed on the fly and do not require storage in  $p^\perp$ . Figure 10 shows an example of coboundary matrices for edges and triangles. The triangle  $t = \langle ab, c \rangle$  will be in the coboundary of exactly three edges (see figure 10a). Since the diameter of  $t$  is  $\{a, b\}$ , the row of  $t$  will have all zeroes to the left of  $(\langle ab, c \rangle, ab)$ . If additionally,  $t$  is the smallest simplex in the coboundary of  $\{a, b\}$ , then there will be all zeroes below  $(\langle ab, c \rangle, ab)$ . Consequently,  $(\langle ab, c \rangle, ab)$  will be a persistence pair and will not require any reduction. We will call such pairs *trivial persistence pairs*, and we will not store them in  $p^\perp$ . Instead, during the reduction of  $r$ , we check whether  $\delta_* = \langle k_1, k_2 \rangle$  is the smallest simplex in the coboundary of the edge  $e' = f_1^{-1}(k_1)$ ; if true, then  $(\delta_*, e')$  is a trivial persistence pair and the next reduction is to be with exactly the coboundary of  $e'$  (since trivial persistence pairs do not require any reductions). Note that paired-indexing gives direct access to the diameter of  $t$  as its primary key, reducing the computation time. For further optimization, the smallest simplex in the coboundary of each edge is stored a priori at the cost of  $O(n_e)$  memory.

Similarly, a tetrahedron,  $h = \langle ab, cd \rangle$ , will be in the coboundary of exactly four triangles (see figure 10b). The greatest triangle in the boundary of  $h$  will be  $t = \langle ab, \max\{c, d\} \rangle$ . Following similar reasoning, if  $h$  is the smallest simplex in the coboundary of  $t$ , then we say that  $(h, t)$  is a trivial persistence pair. During reduction of any triangle, we check whether  $\delta_* = \langle k_1, k_2 \rangle$  is the smallest simplex in the coboundary of the triangle  $t' = \langle k_1, \max\{f_1^{-1}(k_2)\} \rangle$ ; if true,  $(\delta_*, t')$  is a trivial persistence pair and the next reduction is to be with the coboundary of  $t'$ . `FindSmallesth` is used to check whether  $\delta_*$  is the smallest simplex in  $\delta t'$ .

## 4.4 Parallelizing: A general serial-parallel reduction algorithm

To reduce the computation time, we parallelized the function `ReduceV` in algorithm 3, by distributing the processing of edges in  $v$  across multiple threads. An algorithm similar to algorithm 3 can be designed to reduce the triangles and compute the persistence pairs in  $H_2^*$ . However, unless the filtration is very sparse, the number of triangles to be processed to compute  $H_2^*$  is generally significantly larger than the number of edges to be processed to compute  $H_1^*$ ; and parallelizing `ReduceV` does not provide significant improvements. We developed a novel serial-parallel algorithm that can reduce multiple simplices in parallel. In essence, rather than reducing one simplex at a time, we will reduce a batch of simplices. Any algorithm cannot be embarrassingly parallel because of the inherent order in reduction imposed by the filtration. We introduce the serial-parallel algorithm by parallelizing the standard column algorithm (algorithm 1) for cohomology computation (see figure 13).

Parallel (figure 11a): Suppose  $R^\perp$  contains reductions of the first  $n$  edges in  $F^{-1}$ . Let  $\mathbf{r} = [r_1, \dots, r_B]$  be the batch of next  $B$  edges in  $F_1^{-1}$  that have to be reduced. Initially, each  $r_i$  is the coboundary of the corresponding edge, and during reduction it contains the result of the ongoing reduction. Then, if the low of  $r_i$  and  $r_j$  in  $\mathbf{r}$  is equal to that of  $R^\perp(e)$  for

---

**Algorithm 3** Implicit row algorithm (edges)—does not store  $r$ ; does not store diagonal elements of  $V^\perp$ ; and does not store trivial persistence pairs in  $p^\perp$

---

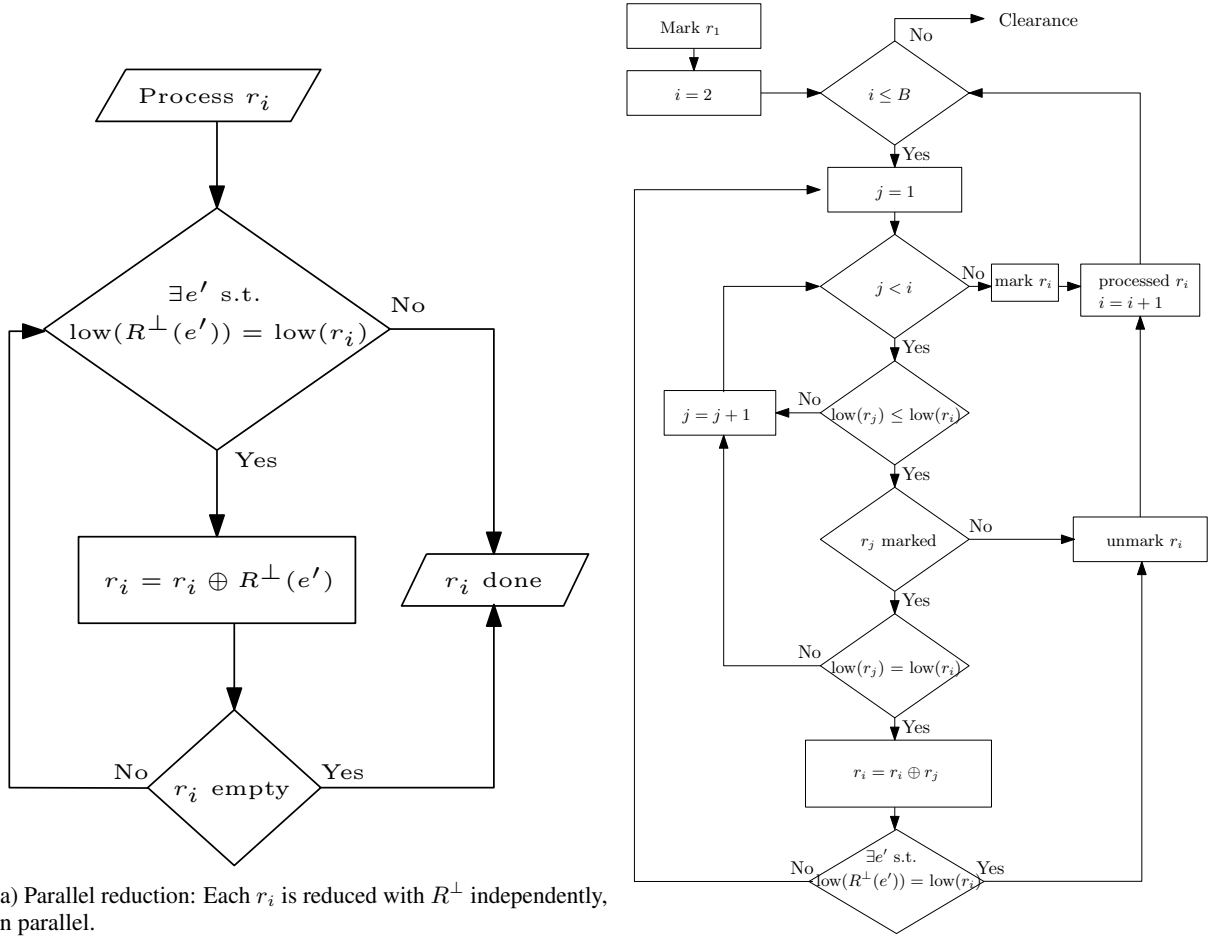
```

1: Input:  $F_1$ 
2: Output:  $p^\perp$ 
3:  $V^\perp, p^\perp$  are empty
4: for  $e$  in  $F_1^{-1}$  do
5:    $(e, i_a, i_b, \delta_e) \leftarrow \text{FindSmallestt}(e)$ 
6:    $\delta_* \leftarrow \delta_e$ 
7:   if primary key of  $\delta_*$  is  $e$  then
8:      $(\delta_*, e)$  is a trivial persistence pair; continue
9:    $v \leftarrow [(e, i_a, i_b, \delta_e)]$ 
10:  while  $\delta_*$  not empty AND  $((\delta_*, e')$  is trivial pers. pair OR is in  $p^\perp)$  do
11:    Append  $\text{FindGEQt}(\delta_*, e')$  to  $v$ 
12:    for  $e''$  in  $V^\perp(e')$  do
13:      Append  $\text{FindGEQt}(\delta_*, e'')$  to  $v$ 
14:     $v, \delta_* \leftarrow \text{ReduceV}(v, \delta_*)$ 
15:    if  $\delta_*$  not empty then
16:       $V^\perp(e) \leftarrow$  edges (not  $e$ ) in  $v$  with non-zero coefficient
17:       $p^\perp \leftarrow (\delta_*, e)$ 
18: Function  $\text{ReduceV}$ 
19:  Input:  $v, \delta_*$ 
20:  Output:  $v, \delta_*$ 
21:  coeff  $\leftarrow 0$ 
22:  while coeff = 0 do
23:     $\delta \leftarrow \text{MAX}$ 
24:    for  $\phi_e = (e, i_a, i_b, \delta_e)$  in  $v$  do
25:      if  $\delta_e$  is Empty OR  $\delta_e > \delta$  then
26:        continue
27:      if  $\delta_e = \delta_*$  then
28:         $(e, i_a, i_b, \delta_e) \leftarrow \text{Function FindNextt}((e, i_a, i_b, \delta_e))$ 
29:      if  $\delta_e < \delta$  then
30:         $\delta \leftarrow \delta_e$ 
31:        coeff  $\leftarrow 1$ 
32:      else if  $\delta_e = \delta$  then
33:        coeff  $\leftarrow 1 - \text{coeff}$ 
34:     $\delta_* \leftarrow \delta$ 
35:    if  $\delta_* = \text{MAX}$  then
36:      return  $v$ , Empty
37:  return  $v, \delta_*$ 

```

---

some edge  $e$ , reducing  $r_i$  and  $r_j$  with  $R^\perp(e)$  will take precedence over reducing them with each other. As a result, each  $r_i$  can be reduced with  $R^\perp$  in parallel.



(a) Parallel reduction: Each  $r_i$  is reduced with  $R^\perp$  independently, in parallel.

(b) Serial reduction: After parallel reduction, columns in  $\mathbf{r}$  are reduced with each other.

Figure 11: Flowcharts for parallel and serial reductions that form the serial-parallel algorithm.

**Serial** (figure 11b): After  $\mathbf{r}$  has been reduced with  $R^\perp$ , we reduce the columns in  $\mathbf{r}$  with each other using *serial reduction*. We ‘mark’  $r_i$  if it is completely reduced. After parallel reduction, none of the  $r_i$  have the same low as any column in  $R^\perp$ . Hence,  $r_1$  is completely reduced and we mark it. Then, carrying out the standard column algorithm, the low of every  $r_i$  ( $i > 1$ ) is compared sequentially with  $r_j$  for every  $j < i$ . We consider the following cases for every  $r_j$ . (1) If  $\text{low}(r_j) > \text{low}(r_i)$ , then we skip it. (2) Otherwise, we check whether  $r_j$  is marked. (2a) If it is unmarked, we cannot continue reduction of  $r_i$  before reducing  $r_j$  so we unmark  $r_i$  and increment  $i$  by one. (2b) If  $r_j$  is marked and  $\text{low}(r_j) = \text{low}(r_i)$ , then we reduce  $r_i$  with  $r_j$ , and we check whether the new low of  $r_i$  is also the low of a column in  $R^\perp$ . If true, then  $r_i$  has to be reduced with  $R^\perp$  before reducing with any  $r_j$  in  $\mathbf{r}$ ; and we unmark  $r_i$  and increment  $i$  by one. Otherwise, if the updated low is not the low of any column in  $R^\perp$ , then  $j \rightarrow 1$ . This process is repeated to reduce  $r_i$  until either  $j$  reaches  $i$  or  $r_i$  is unmarked. When all of  $\mathbf{r}$  has been processed, i.e.,  $i$  reaches the end of  $\mathbf{r}$ , we go to clearance. A detailed hypothetical example is shown in figure 12.

**Clearance**: All marked  $r_i$  are appended to  $R^\perp$ , freeing up space in  $\mathbf{r}$  to be filled in by the coboundaries of the next edges from  $F_1^{-1}$ . After filling  $\mathbf{r}$  with the new coboundaries, we go back to parallel reduction. This process is continued until all edges in  $F_1^{-1}$  have been reduced. The structure of the algorithm is shown in figure 13.

In Dory, we implement the serial-parallel algorithm to reduce coboundaries of triangles (computing  $H_2^*$ ) and we use the implicit row reduction—the batch to be reduced is represented by  $\mathbf{v} = [v_1, \dots, v_B]$ , and we store  $V^\perp$  and  $p^\perp$ . Then, reducing  $r_i$  with  $R^\perp$  is implemented using the implicit row algorithm using  $v_i$  and  $V^\perp$ , as shown earlier. The implicit

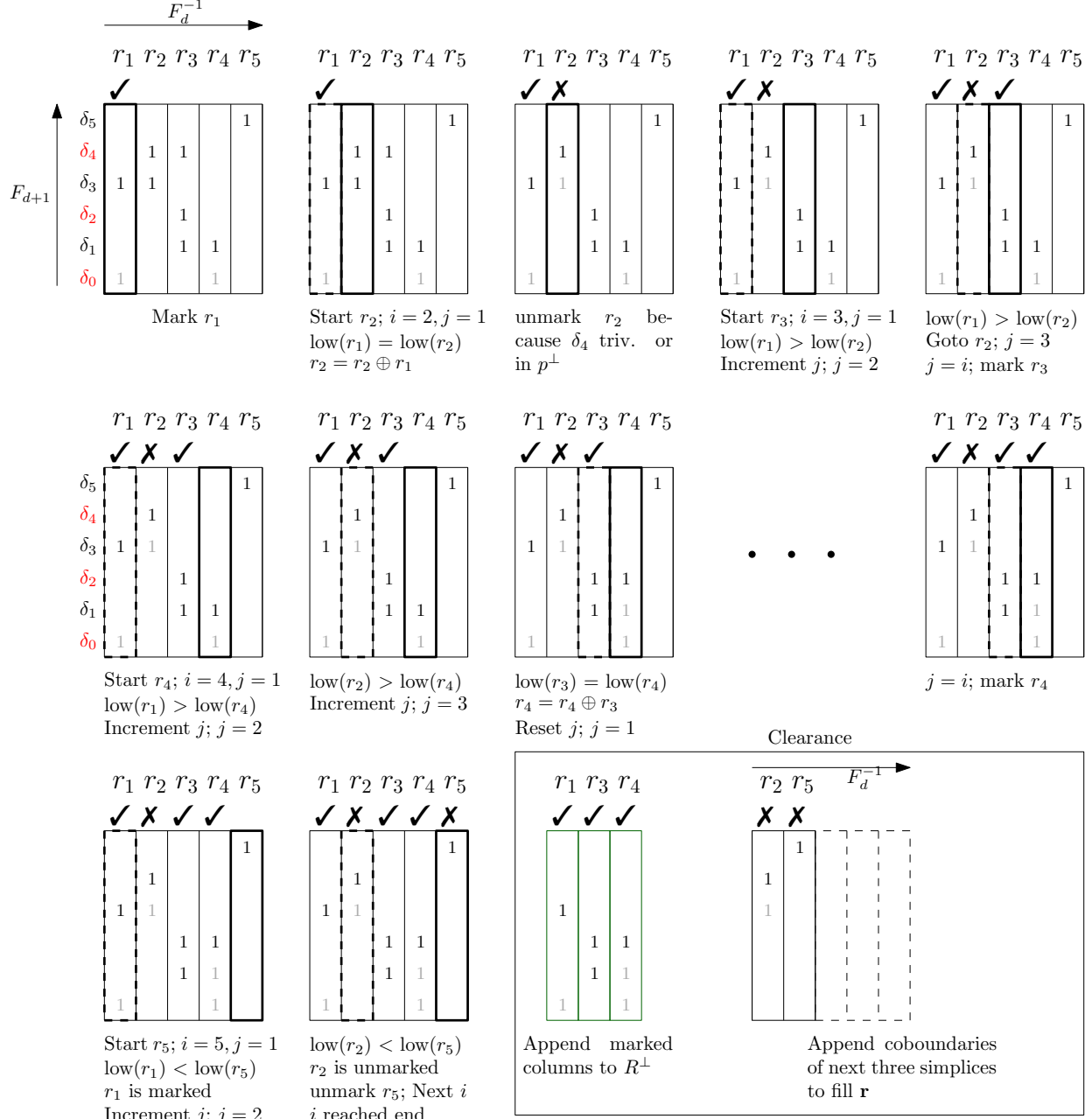


Figure 12: Hypothetical example to illustrate serial reduction in serial-parallel algorithm. The simplices marked by red indicate that they are in a persistence pair in  $p^\perp$ .



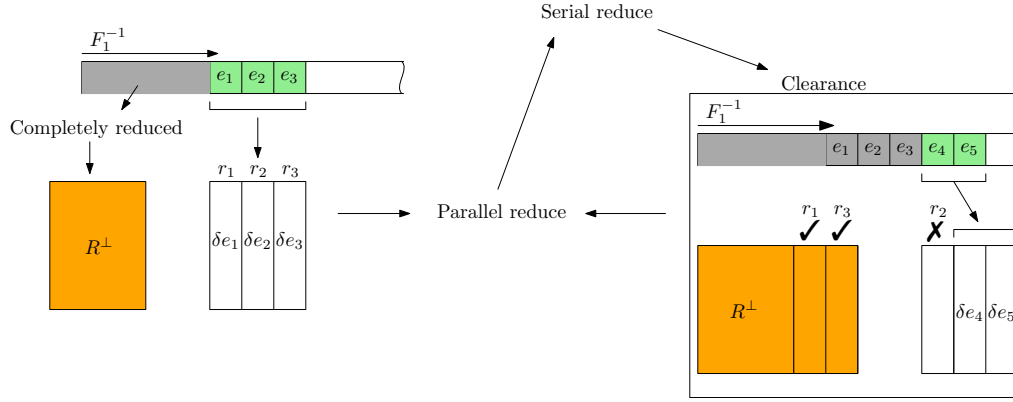


Figure 13: Serial-parallel algorithm to reduce coboundaries of edges. Similar algorithm structure is used to parallelize reduction of coboundaries of triangles ( $H_2^*$ ) and to reduce boundaries of edges ( $H_0$ ).

reduction of  $r_i$  with  $r_j$  using  $v_i$  and  $v_j$  is modified slightly because  $v_j$  stores the  $\phi$ -representations and `FingGEQh` is not required when appending  $v_j$  to  $v_i$ . Additionally, trivial persistence pairs are not stored and are computed on the fly in the parallel reduction. The modified flowcharts are shown in figure 14. For different scenarios during serial reduction, we use four different flags for every  $r_i$ — $f_v$  flags whether  $r_i$  has to be reduced with a trivial persistence pair;  $f_r$  flags whether  $r_i$  is to be reduced with  $R^\perp$ ;  $f_a$  is flagged if it is completely reduced; and  $f_e$  is flagged if  $r_e$  is empty. Note that flagging  $f_v$  and  $f_r$  is similar to unmarking  $r_i$ , and flagging  $f_a$  is similar to marking  $r_i$ . The basic flow of the serial-parallel algorithm to reduce triangles is shown in algorithm 4. See appendix D for pseudocode of serial (algorithm 19) and parallel (algorithm 18) reduction. We also use the serial-parallel algorithm to parallelize standard column algorithm to compute  $H_0$ .

---

**Algorithm 4** SerialParallel: Reduction of triangles

---

```

1: Function SerialParallelReduce
2:   Function ParallelReduce
3:   Function SerialReduce
4:   Function Clearance
5: EndFunction

6: Input  $F_1$ , batch-size
7:  $V^\perp, \mathbf{v} \leftarrow []$ 
8:  $i \leftarrow 0$ 
9: for  $e$  in  $F_1^{-1}$  do
10:   Compute  $\delta e$  and sort it along  $F_2^{-1}$ 
11:   for  $t$  in  $\delta e$  with  $d(t) = e$  do
12:      $(t, i_a, i_b, i_c, f, \delta_t) \leftarrow$  Function FindSmallesth( $t$ )
13:     if  $\delta_1^t$  is Empty then
14:       continue
15:      $v_i \leftarrow [(t, i_a, i_b, i_c, f, \delta_t)]$ 
16:      $\delta_*^{v_i} \leftarrow \delta_t$ 
17:      $f_e \leftarrow 0$ 
18:     Append  $(t, v_i, \delta_*^{v_i}, f_v, f_r, f_a, f_e)$  to  $\mathbf{v}$ 
19:      $i \leftarrow i + 1$ 
20:     if  $i =$  batch-size then
21:       Function SerialParallelReduce

22: while  $i > 0$  do
23:   Function SerialParallelReduce

```

---

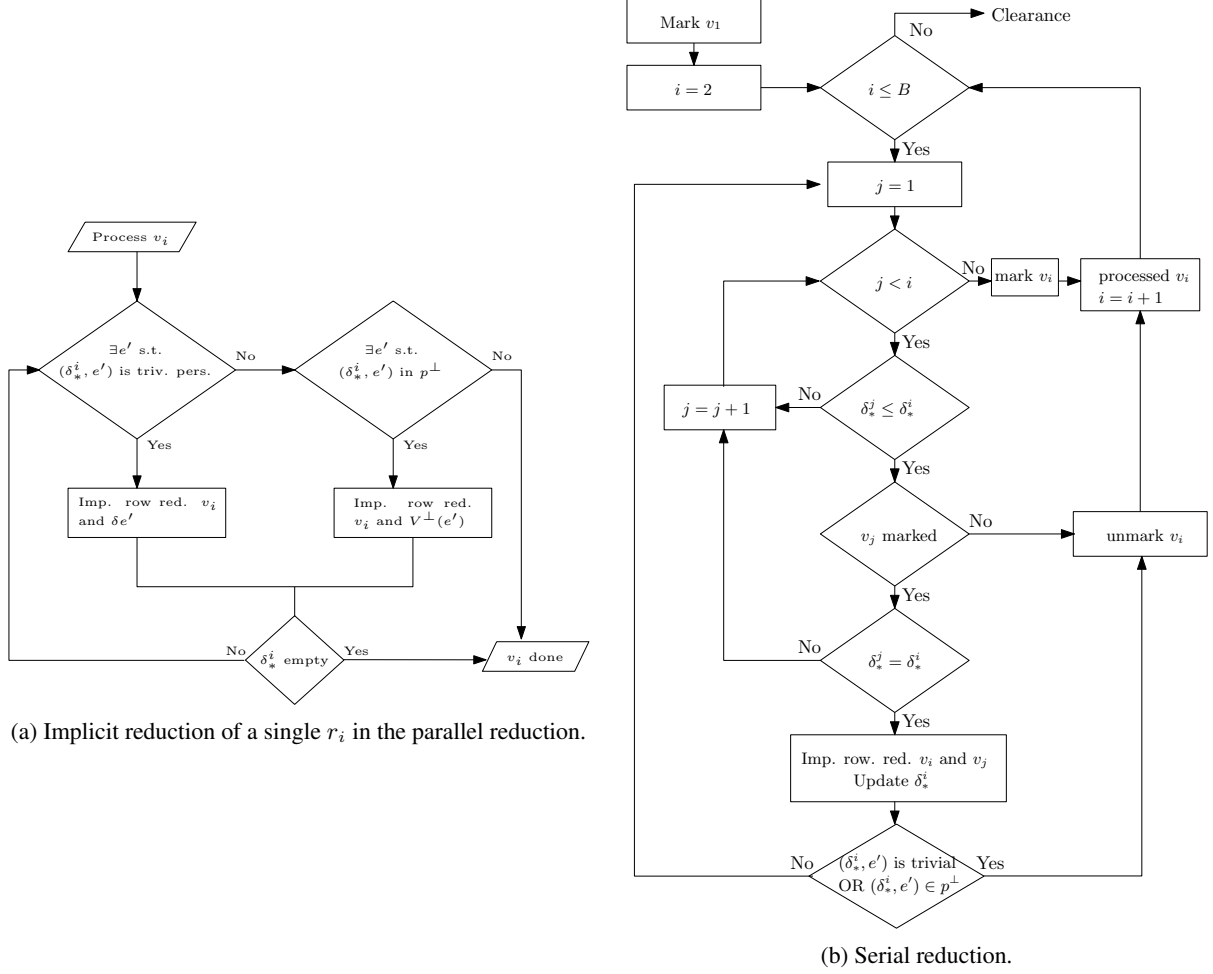


Figure 14: Flowcharts for algorithms in serial-parallel reduction using implicit row reduction and incorporating trivial persistence pair computation.

#### 4.5 All together with clearing strategy

We summarize the algorithm to compute the persistence pairs for groups  $H_0$ ,  $H_1^*$ , and  $H_2^*$  in algorithm 5, including the clearing strategy suggested by Chen and Kerber [2011]. This strategy provides significant reduction in computation time of cohomology reduction by eliminating the need for reduction of certain simplices. In essence, if  $(\tau, \sigma)$  is a persistence pair in  $H_d$  (or  $(\sigma, \tau)$  is in  $H_d^*$ ), then there cannot exist a persistence pair  $(\sigma, \omega)$  in  $H_{d+1}$ . Consequently, there cannot exist a pair  $(\omega, \sigma)$  in  $H_{d+1}^*$ , and there is no need to reduce the coboundary of  $\sigma$  when computing  $H_{d+1}^*$ .

#### 4.6 Sparse vs. non-Sparse

In the case of non-sparse filtrations, our experiments showed that most of the computation time was being spent on the binary search in edge- and vertex-neighborhoods to find orders of the edges during cohomology computation. We implemented an alternate version in which we use combinatorial indexing to store the orders of all the edges in the filtration. This reduces computation time by replacing binary search by an array access at the cost of using  $O(n^2)$  memory instead of  $O(n_e^2)$ . We call the non-sparse version Dory and the sparse version DoryS. In most cases it is advisable to use DoryS because the reduction in memory use outweighs the computation cost. Dory should be considered when computing  $H_2$  for non-sparse filtrations.

**Algorithm 5** Computing all

---

```

1: Input:  $F_1$ 
2: Output: Persistence pairs in  $H_0, H_1^*, H_2^*$ 
3:
4: for  $e$  in  $F_1$  do ▷ Compute  $H_0$ 
5:   Serial-Parallel reduction
6:
7: for  $e$  in  $F_1^{-1}$  do ▷ Compute  $H_1^*$ 
8:   if  $e$  is in a persistence pair in  $H_0$  then ▷ Clearing strategy
9:     continue
10:  Reduction
11:
12: for  $e$  in  $F_1^{-1}$  do ▷ Compute  $H_2^*$ 
13:   for  $t$  in  $\delta e$  with  $d(t) = e$  do
14:     if  $t$  is in a persistence pair in  $H_1^*$  then ▷ Clearing strategy
15:       continue
16:   Serial-parallel reduction

```

---

Data set	$n$	$\tau_m$	sparsity	$d$	$N$	Gudhi	Eirene	Ripser	Dory/DoryS
dragon	2000	$\infty$	1	1	1333335000	✗	✓	✓	✓
fract	512	$\infty$	1	2	2852247169	✗	✓	✓	✓
o3	8192	1	0.0098	2	33244954	✓	✓	✗/✓	✓
torus4(1)	50000	0.15	0.0018	1	41629821	✓	✓	✓	✓
torus4(2)	50000	0.15	0.0018	2	454608895	✓	✗	✗	✓

Table 1: The data sets to benchmark the algorithms. Sparsity is the ratio of the permissible edges in the filtration to the total possible edges. Only Dory and DoryS are able to process all of these data sets within 600 sec. Ripser’s results for o3 are inconsistent with results from other algorithms.

## 5 Computational experiments

We compare the memory taken and the computation time with Gudhi, Eirene, and Ripser. We use four data sets—dragon, fractal, o3, and torus4 (Table 1). All computations are done on a computer with a 2.4 GHz 8-Core Intel Core i9 processor and 64 GB memory. Dory and DoryS are the only algorithms that were able to compute PH for all of these data sets in less than 600 sec. To compare the performance of the algorithms in both computation time and memory requirement, we plot the results across both these benchmarks for every data set in figure 15. The complete tables are in appendix E.

The results show that for every data set either Dory or DoryS is closest to the origin. In all cases they require significantly less memory. In addition, the 4-threaded execution is computationally the fastest in all cases except for one, o3, for which Ripser is faster. However, we observe significant discrepancies in the PD for the third dimension computed by Ripser for this data set compared to other algorithms (figure 16c). Since PDs from Dory are consistent with Eirene and Gudhi (figures 16b and 16a), we suspect that Ripser’s faster computation for this data set is an anomaly. All the PDs are shown in appendix F.

## 6 Topology of human genome

Among different techniques to quantify chromatin structure, Hi-C experiments allow relatively unbiased measurements across an entire genome [Lieberman-Aiden et al., 2009]. Hi-C is based on chromosome conformation capture (3C) which attempts to determine spacial proximity in the cell nucleus between pairs of genetic loci. The experiments measure the interaction frequency of every pair of loci on the genome, and this is believed to correlate with spacial distance in the cell nucleus [Lieberman-Aiden et al., 2009, Dixon et al., 2012].

Using Hi-C experiments, Rao et al. [2014] identified chromatin loops in mouse lymphoblast cells which are orthologous to loops in human lymphoblastoid cells. To highlight the functional importance of chromatin loops they provide multiple sources of evidence that associate most of the detected loops with gene regulation. In Rao et al. [2017] they showed that treatment of DNA with auxin removes most loop domains.

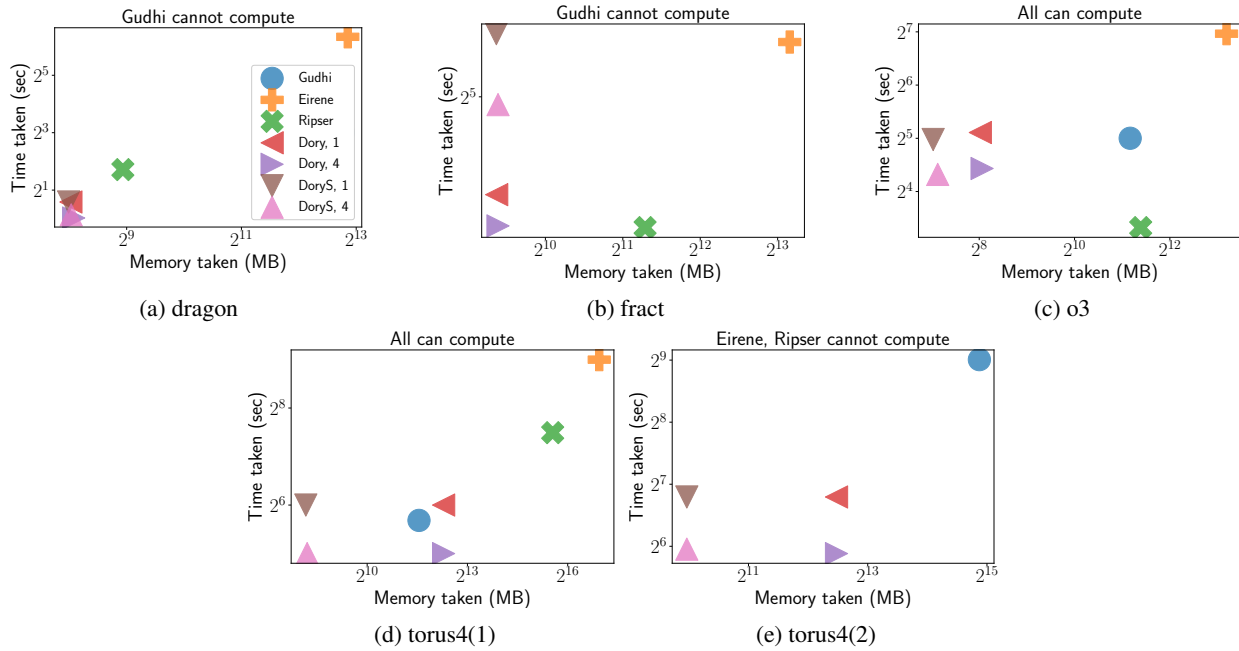


Figure 15: Comparing memory and computation time across different algorithms for the data sets. Dory and/or DoryS outperform all of the algorithms for all of the data sets (closest to the origin in all of the cases). Ripser has a faster computation for o3, but the resulting PD is inconsistent.

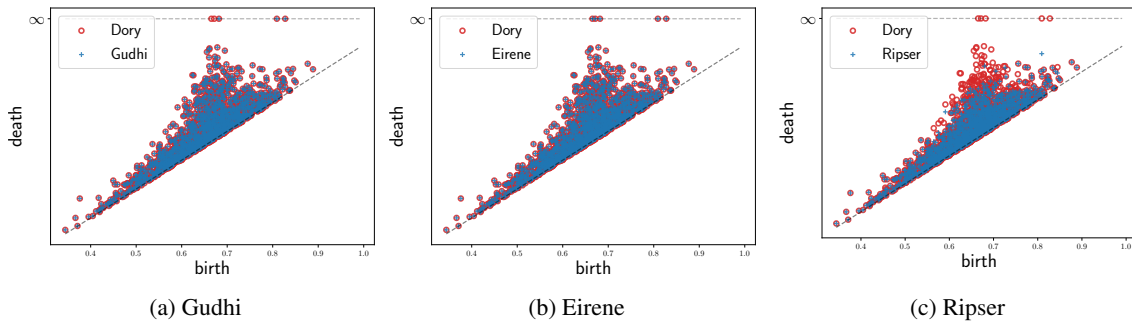


Figure 16: Comparing the persistence diagrams in the third dimension ( $H_2$ ) for data set o3. Dory and Eirene match perfectly. Gudhi differs only by two features that do not die; this difference can be attributed to floating-point arithmetic. Ripser computes a significantly different topology.

We test this result by computing PH to compare the number of loops (and voids) across the Hi-C data sets from two different experimental conditions—with and without auxin treatment, provided in Rao et al. [2017]. To compute PH, the DNA is visualized as a point-cloud where each point represents a contiguous segment of a 1000 base pairs on a chromosome, a so-called genomic bin. The relative pairwise spatial distances between genomic bins are then estimated from the Hi-C data set at this 1 kilobase resolution. The functionally significant loops in this point-cloud are most likely the ones with spacially close genomic bins on their boundary to allow for biological interaction via physical processes such as diffusion. Therefore, we compute PH up to a low  $\tau_m$  resulting in a sparse filtration. When computing PH for this sparse filtration, the published algorithms ran out of memory either because they did not have a provision to accept a sparse filtration or because of their memory requirement during the computation. Dory computed the PH in around 525 sec, taking at most 9.35 GB of computer memory. The PD for dimension 1 shows a significant decrease in the number of loops in the auxin-treated data set (see figure 17a), corroborating previous results. Additionally, Dory reveals that the number of three-dimensional topological features (voids) decreases significantly upon addition of auxin (see figure 17b), which warrants an investigation into possible biological implications. The PDs are shown in appendix G.

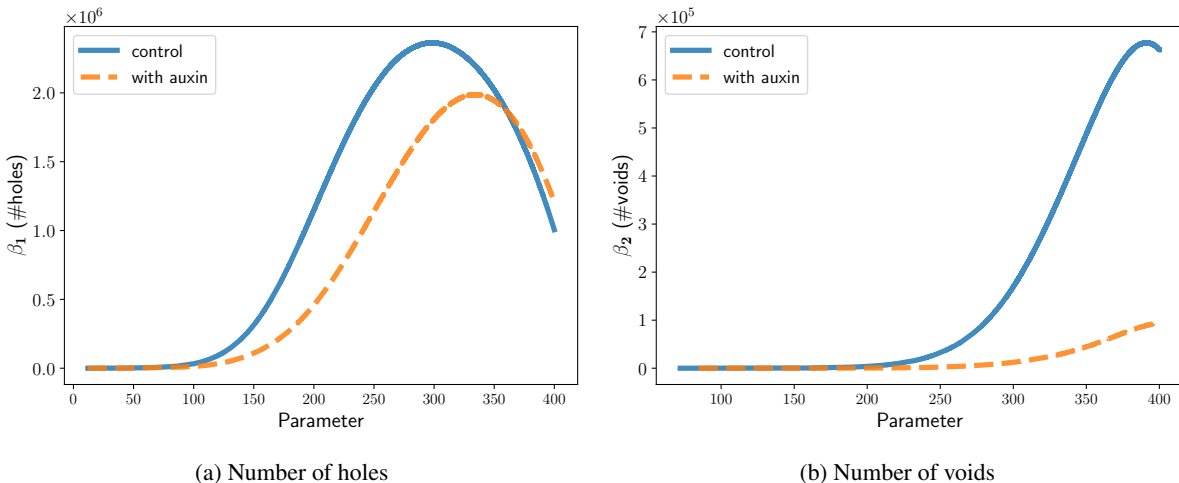


Figure 17: PH of the entire human genome at 1 kilobase resolution shows that the number of loops and voids decreases significantly upon addition of auxin.

## 7 Discussion

In this paper we introduced a new algorithm that overcomes computational limitations that have prevented the application of PH to large data sets. Compared with pre-existing algorithms, Dory provides significant improvements in memory requirements, without an impractical increase in the computation time. Dory is able to process the large Hi-C data set for the human genome at high resolution, corroborating the expected topology changes of chromatin in different experimental conditions.

While our algorithm is limited to computing PH for VR-filtrations up to three dimensions, a large class of real-world scientific data sets requires only such dimensional restrictions. The current implementation of the algorithm computes PH modulo 2, but it can be easily extended to any prime field.

An alternate class of methods deals with large data sets by approximating their PDs. For example, SimBa [Dey et al., 2019] reduces the number of simplices in the filtration by approximating it to a sparse filtration such that the PDs of the sparse filtration are within a theoretical error of margin when compared to those of the original filtration. Another method, PI-Net [Som et al., 2020], uses neural networks to predict persistence images, that are pixelated approximations of PDs in  $\mathbb{R}^2$ . The former method uses Gudhi to compute PDs of the approximated sparse filtrations and the latter uses Ripser to compute true PDs when training the neural network. Since Dory can handle larger data sets compared to both Gudhi and Ripser, SimBa and PI-Net can expand their scope by using Dory instead.

We showed that Dory outperforms published algorithms in both memory requirement and computation time for the data sets in table 1. Dory will consistently require the least amount of memory because of paired-indexing and implicit row reduction, but its computation time is sensitive to the number of reduction operations required to process a data set. As an example, we computed PH for 30 randomly generated data sets with the same number of points and similar PDs. The data set with fastest computation by Dory took ( $\approx 4$  sec,  $\approx 300$  MB) and the slowest took ( $\approx 1800$  sec,  $\approx 300$

MB). In contrast, for these two data sets, Ripser took ( $\approx 4$  sec,  $\approx 800$  MB) and ( $\approx 35$  sec,  $\approx 2900$  MB), respectively. This illustrates a potential trade-off between reducing memory requirement and increasing computation time in the current version of Dory. We are exploring ways to improve on this trade-off.

In this paper we have focused on computing PDs. However, our algorithm can also be extended to compute representative boundaries of the holes and voids in the data set. For scientific applications, these representative boundaries of topological features in the data set are critical for connecting topology to structural properties of the data that may be linked to functional properties of the underlying system. For instance, they might yield insights into the biological implications of reduction in the number of voids in human genome upon treatment with auxin. Computation of representative boundaries faces the hurdle of high memory cost, and we are currently working on developing a scalable algorithm.

# Appendices

## A Standard row and column algorithms

---

### Algorithm 6 Standard column algorithm

---

```

1: for  $j : 2$  to  $N$  do
2:    $i \leftarrow 1$ 
3:   while  $i < j$  do
4:     if  $\text{low}(j) = \text{pivot}(i)$  then
5:        $\text{column } j \leftarrow \text{column } j \oplus \text{column } i$ 
6:       if  $\text{column } j$  is empty then
7:          $\text{low}(j) \leftarrow -1$  ▷ this column is reduced to  $\mathbf{0}$ 
8:         break
9:       else
10:         $i \leftarrow 1$ 
11:      else
12:         $i \leftarrow i + 1$ 
13:       $\text{pivot}(j) \leftarrow \text{low}(j)$ 

```

---



---

### Algorithm 7 Standard row algorithm

---

```

1: for  $i : N$  to  $1$  do
2:   for  $j : 1$  to  $N$  do
3:     if  $\text{low}(j) = i$  then break
4:   if  $j = N + 1$  then continue
5:    $\text{pivot}(j) = \text{low}(j)$ 
6:   for  $k = j + 1$  to  $N$  do
7:     if  $\text{low}(k) = i$  then
8:        $\text{column } k \leftarrow \text{column } k \oplus \text{column } j$ 
9:       if  $\text{column } k$  is empty then
10:         $\text{low}(k) \leftarrow -1$  ▷ this column is reduced to  $\mathbf{0}$ 
11:         $\text{pivot}(k) \leftarrow -1$ 

```

---

## B Algorithms to compute cohomology for edges

---

### Algorithm 8 Case 1 for edges

---

```

1: Input:  $(e, i_a, i_b, \delta_e)$ 
2: Output:  $(e, i_a, i_b, \delta_e)$ 
3:  $\{a, b\} \leftarrow f_1^{-1}(e)$ 
4: while  $i_a < N(a)$  AND  $i_b < N(b)$  do
5:   if  $f_0(n_{i_a}^a) < f_0(n_{i_b}^b)$  then
6:      $i_a \leftarrow i_a + 1$ 
7:   else if  $f_0(n_{i_a}^a) > f_0(n_{i_b}^b)$  then
8:      $i_b \leftarrow i_b + 1$ 
9:   else
10:    return  $(e, i_a, i_b, \langle f_1(\{a, b\}), n_{i_a}^a \rangle)$ 
11: return  $(e, i_a, i_b, \text{Empty})$ 

```

▷ Move to case 2

---

### Algorithm 9 Case 2 for edges

---

```

1: Input:  $(e, i_a, i_b, \delta_e)$ 
2: Output:  $(e, i_a, i_b, \delta_e)$ 
3:  $\{a, b\} \leftarrow f_1^{-1}(e)$ 
4: while  $i_a < N(a)$  AND  $i_b < N(b)$  do
5:   if  $f_1(e_{i_a}^a) < f_1(e_{i_b}^b)$  then
6:      $\{a, d\} \leftarrow f_1^{-1}(e_{i_a}^a)$ 
7:     if  $d \in N^b$  AND  $f_1(\{b, d\}) < f_1(e_{i_a}^a)$  then
8:       return  $(e, i_a, i_b, \langle f_1(e_{i_a}^a), d \rangle)$ 
9:     else
10:       $i_a \leftarrow i_a + 1$ 
11:   else
12:      $\{b, d\} \leftarrow f_1^{-1}(e_{i_b}^b)$ 
13:     if  $d \in N^a$  AND  $f_1(\{a, d\}) < f_1(e_{i_b}^b)$  then
14:       return  $(e, i_a, i_b, \langle f_1(e_{i_b}^b), d \rangle)$ 
15:     else
16:       $i_b \leftarrow i_b + 1$ 
17:   while  $i_a < N(a)$  do
18:      $\{a, d\} \leftarrow f_1^{-1}(e_{i_a}^a)$ 
19:     if  $d \in N^b$  AND  $f_1(\{b, d\}) < f_1(e_{i_a}^a)$  then
20:       return  $(e, i_a, i_b, \langle f_1(e_{i_a}^a), d \rangle)$ 
21:     else
22:       $i_a \leftarrow i_a + 1$ 
23:   while  $i_b < N(b)$  do
24:      $\{b, d\} \leftarrow f_1^{-1}(e_{i_b}^b)$ 
25:     if  $d \in N^a$  AND  $f_1(\{a, d\}) < f_1(e_{i_b}^b)$  then
26:       return  $(e, i_a, i_b, \langle f_1(e_{i_b}^b), d \rangle)$ 
27:     else
28:       $i_b \leftarrow i_b + 1$ 
29: return  $(e, i_a, i_b, \text{Empty})$ 

```

---



**Algorithm 10** FindSmallestt

---

```

1: Input:  $e$ 
2: Output:  $(e, i_a, i_b, \delta_e)$ 
3:  $\{a, b\} \leftarrow f_1^{-1}(e)$ 
4:  $i_a \leftarrow 0$ 
5:  $i_b \leftarrow 0$ 
6:  $\delta_0^e \leftarrow \text{Empty}$ 
7:  $(e, i_a, i_b, \delta_e) \leftarrow \text{Function Case1}((e, i_a, i_b, \delta_e))$ 
8: if  $low$  is Empty then
9:    $i_a \leftarrow$  smallest index s.t.  $f_1(e_{i_a}^a) > f_1(e)$ 
10:   $i_b \leftarrow$  smallest index s.t.  $f_1(e_{i_b}^b) > f_1(e)$ 
11:   $(e, i_a, i_b, \delta_e) \leftarrow \text{Function Case2}((e, i_a, i_b, \delta_e))$ 
12: return  $(e, i_a, i_b, \delta_e)$ 

```

---

**Algorithm 11** FindNextt

---

```

1: Input:  $(e, i_a, i_b, \delta_e)$ 
2: Output:  $(e, i_a, i_b, \delta_e)$ 
3:  $\{a, b\} \leftarrow f_1^{-1}(e)$ 
4:  $\langle k^p, k^s \rangle \leftarrow \delta_i^e$ 
5: if  $k^p = f_1(e)$  then
6:   Increment  $i_a, i_b$  by 1
7:    $(e, i_a, i_b, \delta_{i+1}^e) \leftarrow \text{Function Case1}((e, i_a, i_b, \delta_i^e))$ 
8:   if  $\delta_{i+1}^e$  is Empty then
9:      $i_a \leftarrow$  smallest index s.t.  $f_1(e_{i_a}^a) > f_1(e)$ 
10:     $i_b \leftarrow$  smallest index s.t.  $f_1(e_{i_b}^b) > f_1(e)$ 
11:   else
12:     return  $(e, i_a, i_b, \delta_e)$ 
13: else
14:    $f_1(e_{i_a}^a) < f_1(e_{i_b}^b)$  ? increment  $i_a$  : increment  $i_b$ 
15:    $(e, i_a, i_b, \delta_e) \leftarrow \text{Function Case2}((e, i_a, i_b, \delta_e))$ 
16: return  $(e, i_a, i_b, \delta_e)$ 

```

---

**C Algorithms to compute coboundary of triangles**

**Algorithm 12** FindGEQt

---

```

1: Input:  $e, \delta_{\#}$ 
2: Output:  $(e, i_a, i_b, \delta_e)$ 
3:  $\{a, b\} \leftarrow f_1^{-1}(e)$ 
4:  $\langle k^p, k^s \rangle \leftarrow \delta_{\#}$ 
5: if  $k^p < f_1(e)$  then
6:    $(e, i_a, i_b, \delta_e) \leftarrow \text{Function FindSmallestt}(e)$ 
7:   return  $(e, i_a, i_b, \delta_e)$ 
8: else if  $k^p = f_1(e)$  then
9:    $i_a \leftarrow$  smallest index s.t.  $f_0(n_{i_a}^a) \geq k^s$ 
10:   $i_b \leftarrow$  smallest index s.t.  $f_0(n_{i_b}^b) \geq k^s$ 
11:  if  $f_0(n_{i_a}^a) = f_0(n_{i_b}^b)$  then
12:    return  $(e, i_a, i_b, \langle k^p, f_0(n_{i_a}^a) \rangle)$ 
13:  else
14:     $(e, i_a, i_b, \delta_e) \leftarrow \text{Function FindNextt}((e, i_a, i_b, \text{Empty}))$ 
15:    if  $\delta_e$  is not Empty then
16:      return  $(e, i_a, i_b, \delta_e)$ 
17:   $i_a \leftarrow$  smallest index s.t.  $f_1(e_{i_a}^a) \geq k^p$ 
18:   $i_b \leftarrow$  smallest index s.t.  $f_1(e_{i_b}^b) \geq k^p$ 
19:  if  $\langle k^p, k^s \rangle$  is in  $\delta_e$  then
20:    return  $(e, i_a, i_b, \langle k^p, k^s \rangle)$ 
21:   $(e, i_a, i_b, \delta_e) \leftarrow \text{Function Case2}((e, i_a, i_b, \delta_e))$ 
22:  return  $(e, i_a, i_b, \delta_e)$ 

```

---

**Algorithm 13** Case1 for triangles

---

```

1: Input:  $(t, i_a, i_b, i_c, f, \delta_t)$ 
2: Output: 1 or 0
3:  $\langle k^p, k^s \rangle \leftarrow f_2(t)$ 
4:  $a \leftarrow \min\{f_1^{-1}(k^p)\}$ 
5:  $b \leftarrow \max\{f_1^{-1}(k^p)\}$ 
6:  $c \leftarrow k^s$ 
7: while  $i_c < N(a)$  AND  $f_1(e_{i_c}^c) < k^p$  do
8:    $\{c, d\} \leftarrow e_{i_c}^c$ 
9:   if  $f_1(\{a, d\})$  and  $f_1(\{b, d\})$  are less than  $k^p$  then
10:     $f \leftarrow 0$ 
11:     $\delta_t \leftarrow \langle k^p, f_1(e_{i_c}^c) \rangle$ 
12:    return 1
13:    $i_c \leftarrow i_c + 1$ 
14: return 0

```

---

**Algorithm 14** Case 2 for triangles

---

```

1: Input:  $(t, i_a, i_b, i_c, f, \delta_t)$ 
2:  $\langle k^p, k^s \rangle \leftarrow f_2(t)$ 
3:  $a \leftarrow \min\{f_1^{-1}(k^p)\}$ 
4:  $b \leftarrow \max\{f_1^{-1}(k^p)\}$ 
5:  $c \leftarrow k^s$ 
6: while not reached end of all  $E^a, E^b, E^c$  do
7:    $o_* \leftarrow \min\{f_1(e_{i_a}^a), f_1(e_{i_b}^b), f_1(e_{i_c}^c)\}$  ▷ Exclude indices that reach end of edge-nbd
8:    $\{v_1, d\} \leftarrow f_1^{-1}(o_*)$ 
9:    $\{v_2, v_3\} \leftarrow \{a, b, c\} \setminus \{v_1\}$ 
10:  if  $f_1(\{v_2, d\})$  and  $f_1(\{v_3, d\})$  are less than  $o_*$  then
11:     $\delta_t \leftarrow \langle o_*, f_1(\{v_2, v_3\}) \rangle$ 
12:     $f \leftarrow 1$  if  $v_1 = a$ ;  $2$  if  $v_1 = b$ ;  $3$  if  $v_1 = c$ 
13:    return
14:  else
15:    Increment  $i_{v_1}$ 
16:  $\delta_t \leftarrow \text{Empty}$ 
17:  $f \leftarrow -1$ 

```

---

**Algorithm 15** FindSmallesth

---

```

1: Input:  $(t, i_a, i_b, i_c, f, \delta_t)$ 
2:  $i_c \leftarrow 0$ 
3: if Function Case1 $(t, i_a, i_b, i_c, f, \delta_t)$  then
4:   return
5:  $\langle k^p, k^s \rangle \leftarrow t$ 
6:  $\{a, b\} \leftarrow f_1^{-1}(k^p)$ 
7:  $i_a \leftarrow \underset{i_a}{\operatorname{argmin}}(f_1(e_{i_a}^a) \geq k^p)$ 
8:  $i_b \leftarrow \underset{i_b}{\operatorname{argmin}}(f_1(e_{i_b}^b) \geq k^p)$ 
9: Increment  $i_a, i_b$ 
10: Function Case2 $(t, i_a, i_b, i_c, f, \delta_t)$ 

```

---

**Algorithm 16** FindNexth for triangles

---

```

1: Input:  $(t, i_a, i_b, i_c, f, \delta_t)$ 
2:  $\langle k^p, c \rangle \leftarrow f_2(t)$ 
3:  $a \leftarrow \min\{f_1^{-1}(k^p)\}$ 
4:  $b \leftarrow \max\{f_1^{-1}(k^p)\}$ 
5:  $c \leftarrow k^s$ 
6: if  $f = 0$  then
7:   Increment  $i_c$ 
8:   if Function Case1 $(t, i_a, i_b, i_c, f, \delta_t)$  then
9:     return
10:   $i_a \leftarrow \underset{i_a}{\operatorname{argmin}}(f_1(e_{i_a}^a) \geq k^p)$ 
11:   $i_b \leftarrow \underset{i_b}{\operatorname{argmin}}(f_1(e_{i_b}^b) \geq k^p)$ 
12:  Increment  $i_a, i_b$ 
13: if Not moving from Case1 then
14:   if  $f = 1$  then
15:      $i_a \leftarrow i_a + 1$ 
16:   else if  $f = 2$  then
17:      $i_b \leftarrow i_b + 1$ 
18:   else if  $f = 3$  then
19:      $i_c \leftarrow i_c + 1$ 
20: Function Case2 $(t, i_a, i_b, i_c, f, \delta_t)$ 

```

---

**Algorithm 17** FindGEQh for triangles

---

```

1: Input:  $(t, i_a, i_b, i_c, f, \delta_t), \delta_{\#}$ 
2:  $\langle k_{\#}^p, k_{\#}^s \rangle \leftarrow \delta_{\#}$ 
3:  $\langle k^p, c \rangle \leftarrow t$ 
4:  $\{a, b\} \leftarrow f_1^{-1}(k^p)$ 
5: if  $k_{\#}^p < k^p$  then
6:   Function FindSmallesth( $t, i_a, i_b, i_c, f, \delta_t$ )
7:   return
8: else if  $k_{\#}^p = k^p$  then
9:    $i_c \leftarrow \operatorname{argmin}_{i_c} (f_1(e_{i_c}^c) \geq k_{\#}^s)$ 
10:  if  $f_1(e_{i_c}^c) = k_{\#}^s$  then
11:     $\delta_t \leftarrow \delta_{\#}$ 
12:     $v \leftarrow 0$ 
13:    return
14:  if Function Case1( $t, i_a, i_b, i_c, f, \delta_t$ ) then
15:    return
16:   $i_a \leftarrow \operatorname{argmin}_{i_a} (f_1(e_{i_a}^a) \geq k^p)$ 
17:   $i_b \leftarrow \operatorname{argmin}_{i_b} (f_1(e_{i_b}^b) \geq k^p)$ 
18:  Increment  $i_a, i_b$ 
19: else
20:   $i_a \leftarrow \operatorname{argmin}_{i_a} (f_1(e_{i_a}^a) \geq k_o^p)$ 
21:   $i_b \leftarrow \operatorname{argmin}_{i_b} (f_1(e_{i_b}^b) \geq k_o^p)$ 
22:   $i_c \leftarrow \operatorname{argmin}_{i_c} (f_1(e_{i_c}^c) \geq k_o^p)$ 
23: while 1 do
24:  Function Case2( $t, i_a, i_b, i_c, f, \delta_t$ )
25:  if  $\delta_t \geq \delta_{\#}$  OR  $\delta_t$  is Empty then
26:    break
27:  if  $f = 1$  then
28:     $i_a \leftarrow i_a + 1$ 
29:  else if  $f = 2$  then
30:     $i_b \leftarrow i_b + 1$ 
31:  else if  $f = 3$  then
32:     $i_c \leftarrow i_c + 1$ 

```

---

**D Algorithms for serial-parallel cohomology reduction of triangles**

**Algorithm 18** Parallel reduction

---

```

1: Input:  $\mathbf{v}, V^\perp, p^\perp$ 
2: Output:  $\mathbf{v}$ 
3: for  $(t, v_i, \delta_*^{v_i}, f_v, f_r, f_a, f_e)$  in  $\mathbf{v}$  do ▷ Embarrassingly parallel
4:    $f_r \leftarrow 0$ 
5:    $f_a \leftarrow 1$ 
6:   if  $(\delta_*^{v_i}, t)$  is a trivial persistence pair then
7:     continue
8:   while  $(\delta_*^{v_i}, t')$  is a trivial persistence pair OR is in  $p^\perp$  do
9:      $(t', i_a, i_b, i_c, v, \delta_{t'}) \leftarrow \mathbf{Function FindGEQt}(t', \delta_*^{v_i})$ 
10:    Append  $(t', i_a, i_b, i_c, f, \delta_{t'})$  to  $v_i$ 
11:    for  $t_k$  in  $V^\perp(t')$  do
12:       $(t_k, i_a, i_b, i_c, f, \delta_{t_k}) \leftarrow \mathbf{Function FindGEQt}(t_k, \delta_*^{v_i})$ 
13:      Append  $[(t_k, i_a, i_b, i_c, f, \delta_{t_k})]$  to  $v_i$ 
14:    Implicit row algorithm to update  $\delta_*^{v_i}$ 
15:    if  $\delta_*^{v_i}$  is Empty then
16:       $f_e \leftarrow 1$ 
17:    return

```

---

**Algorithm 19** Serial reduction

---

```

1: for  $(t, v_i, \delta_*^{v_i}, f_r^i, f_v^i, f_a^i, f_e^i)$  in  $\mathbf{v}$  do
2:   if  $f_e^i$  OR  $f_v^i$  then
3:     continue
4:    $j \leftarrow 1$ 
5:   while  $j < i$  do
6:     if  $f_e^j$  then
7:        $j \leftarrow j + 1$ 
8:       continue
9:     if  $\delta_*^{v_j} > \delta_*^{v_i}$  then
10:       $j \leftarrow j + 1$ 
11:      continue
12:     if  $\delta_*^{v_j} < \delta_*^{v_i}$  then
13:       if  $f_r^j$  OR  $f_v^j$  then
14:          $f_a^i \leftarrow 0$ 
15:         break
16:        $j \leftarrow j + 1$ 
17:       continue
18:     Append  $v_j$  to  $v_i$ 
19:     Implicit row algorithm to update  $\delta_*^{v_i}$ 
20:     if  $\delta_*^{v_i}$  is Empty then
21:        $f_e^i \leftarrow 1$ 
22:       break
23:     if  $\exists t'$  s.t.  $(\delta_*^{v_i}, t')$  is a trivial pair then
24:        $f_v^i \leftarrow 1$ 
25:        $f_r^i \leftarrow 0$ 
26:        $f_a^i \leftarrow 0$ 
27:       break
28:     if  $(\delta_*^{v_i}, t')$  is a persistence pair in  $p^\perp$  then
29:        $f_v^i \leftarrow 0$ 
30:        $f_r^i \leftarrow 1$ 
31:        $f_a^i \leftarrow 0$ 
32:       break
33:    $j \leftarrow 1$ 

```

---

**Algorithm 20** Clearance

---

```

1: for  $(t, v_i, \delta_*^{v_i}, f_v, f_r, f_a, f_e)$  in  $\mathbf{v}$  do
2:   if  $f_e = 0$  then
3:     Non-contractible cycle born at  $t$ 
4:     Remove  $(t, v_i, \delta_*^{v_i}, f_v, f_r, f_a, f_e)$  from  $\mathbf{v}$ 
5:     continue
6:   if  $f_a \neq 1$  then
7:     Store  $(\delta_*^{v_i}, t)$  in  $p^\perp(t)$ 
8:     Define  $T \leftarrow [t_k \text{ in } v_i = [(t_k, i_a, i_b, i_c, f, \delta_*^{t_k})]]$  with  $t_k \neq t$ 
9:     Remove triangles from  $T$  that occur even number of times (modulo 2 sum)
10:     $V^\perp(t) \leftarrow T$ 
11:    Remove  $(t, v_i, \delta_*^{v_i}, f_v, f_r, f_a, f_e)$  from  $\mathbf{v}$ 

```

---

**E Tables with benchmarks**

Data set	$n$	$\tau_m$	non-sparsity	$d$	Gudhi	Eirene	Ripser	Dory		DoryS	
								1 thd.	4 thds.	1 thd.	4 thds.
dragon	2000	$\infty$	1	1	NA	7.4 GB	489 MB	261 MB	270 MB	254 MB	262 MB
fract	512	$\infty$	1	2	NA	9.13 GB	2.5 GB	662 MB	670 MB	660 MB	670 MB
o3	8192	1	0.0098	2	2.3 GB	9.34 GB	2.68 GB	260 MB	267 MB	131 MB	140 MB
torus4(1)	50000	0.15	0.0018	1	3 GB	126 GB	48 GB	5 GB	5 GB	287 MB	295 MB
torus4(2)	50000	0.15	0.0018	2	30 GB	NA	NA	5.7 GB	5.7 GB	1 GB	1 GB

Data set	$n$	$\tau_m$	non-sparsity	$d$	Gudhi	Eirene	Ripser	Dory		DoryS	
								1 thd.	4 thds.	1 thd.	4 thds.
dragon	2000	$\infty$	1	1	NA	81 s	3.28 s	1.5 s	1.02 s	1.5 s	1.1 s
fract	512	$\infty$	1	2	NA	38.5 s	20.58 s	23 s	20.7 s	39.6 s	31.17 s
o3	8192	1	0.0098	2	32.02 s	125 s	10 s	34.5 s	21.6 s	31.5 s	20 s
torus4(1)	50000	0.15	0.0018	1	51.4 s	511 s	180 s	64 s	32 s	64 s	32 s
torus4(2)	50000	0.15	0.0018	2	514.7 s	NA	NA	111 s	59 s	111 s	62 s

**F Persistence diagrams for data sets**

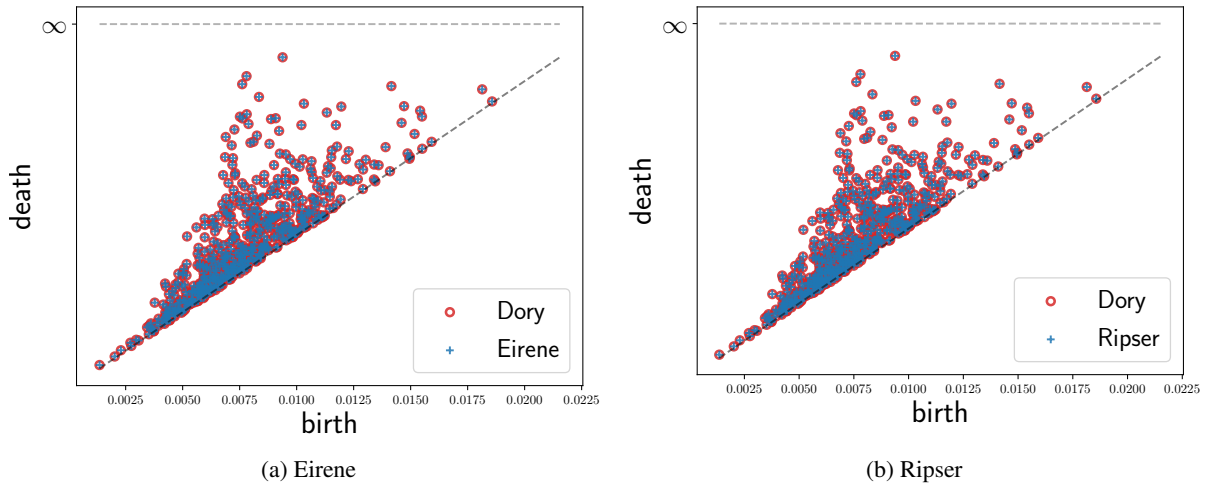


Figure 18: Dragon  $H_1$  PD

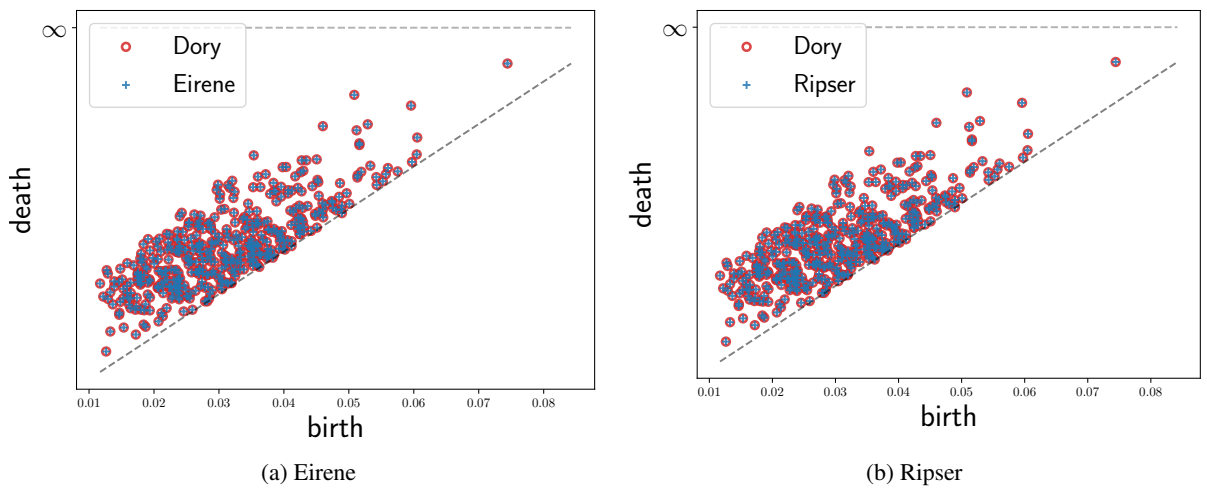


Figure 19: Fractal  $H_1$  PD

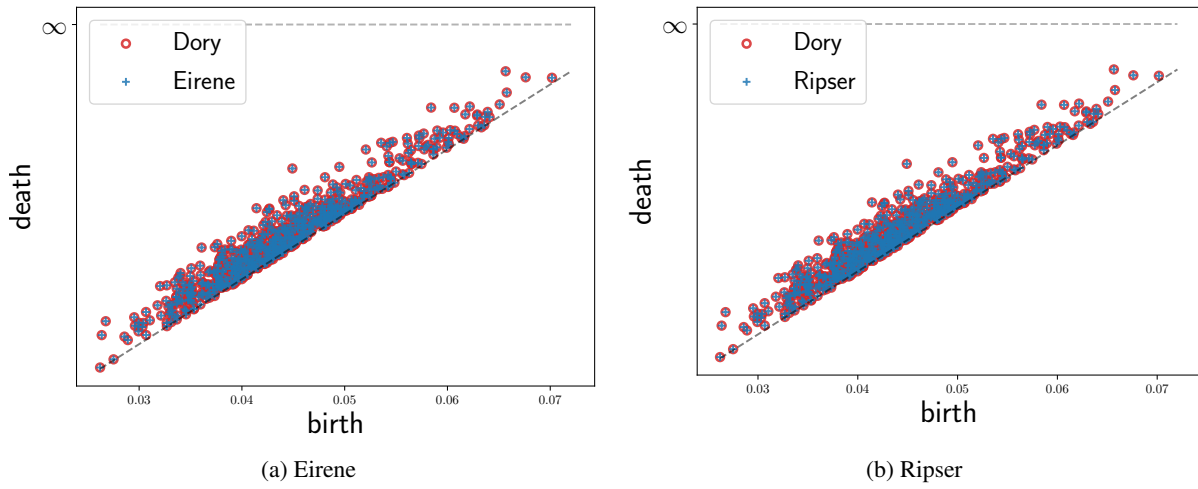


Figure 20: Fractal  $H_2$  PD

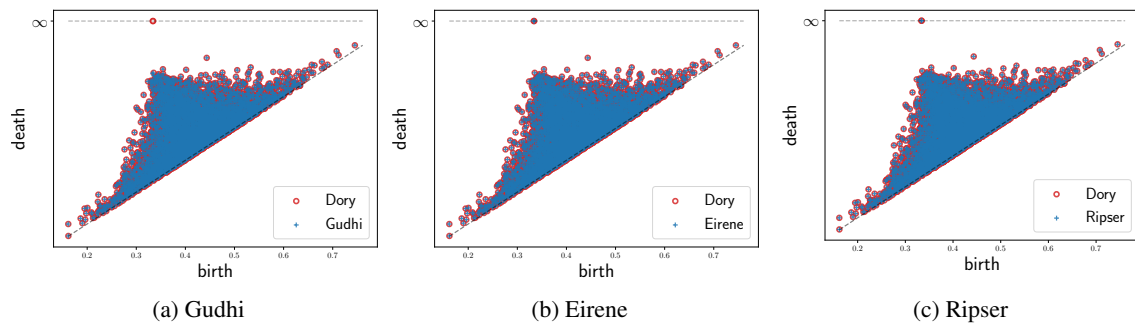


Figure 21:  $o_3 H_1$  PD

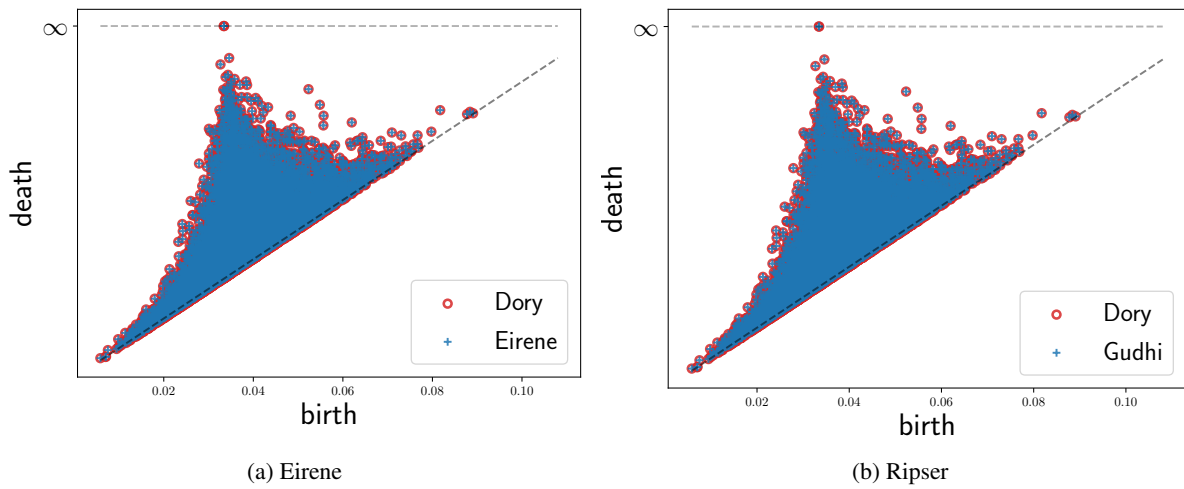
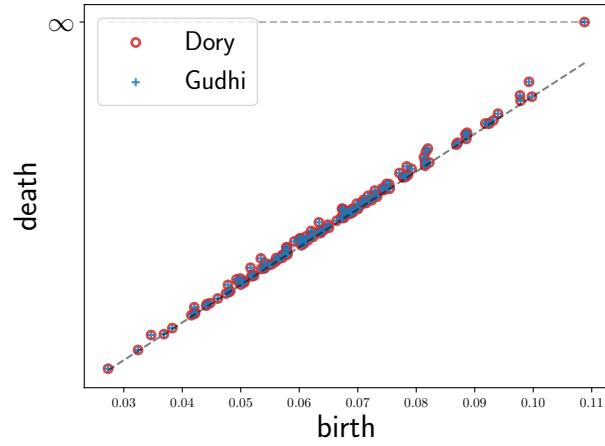
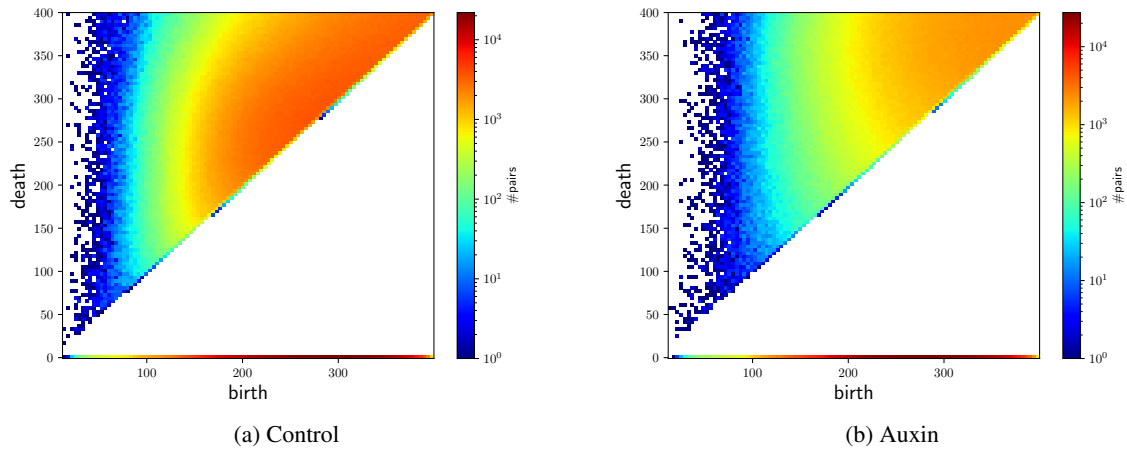


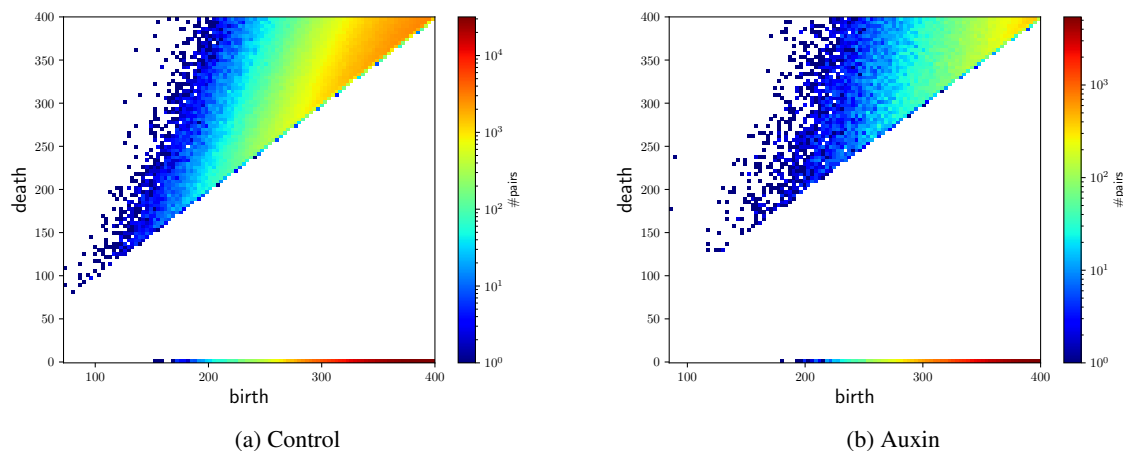
Figure 22: Torus4  $H_1$  PD



Figure 23: Torus4  $H_2$  PD

## G Persistence diagrams for Hi-C

Figure 24: Hi-C data set  $H_1$  PD

Figure 25: Hi-C data set  $H_2$  PD

## References

- Herbert Edelsbrunner and John Harer. Persistent homology—a survey. *Contemporary mathematics*, 453:257–282, 2008.
- Vin De Silva, Dmitriy Morozov, and Mikael Vejdemo-Johansson. Dualities in persistent (co) homology. *Inverse Problems*, 27(12):124003, 2011.
- Jean-Daniel Boissonnat and Clément Maria. The simplex tree: an efficient data structure for general simplicial complexes. *Algorithmica*, 70(3):406–427, 2014.
- Ulrich Bauer. Ripser: efficient computation of vietoris-rips persistence barcodes. *arXiv preprint arXiv:1908.02518*, 2019.
- M Jordan Rowley and Victor G Corces. Organizational principles of 3d genome architecture. *Nature Reviews Genetics*, 19(12):789–800, 2018.
- Erez Lieberman-Aiden, Nynke L Van Berkum, Louise Williams, Maxim Imakaev, Tobias Ragozy, Agnes Telling, Ido Amit, Bryan R Lajoie, Peter J Sabo, Michael O Dorschner, et al. Comprehensive mapping of long-range interactions reveals folding principles of the human genome. *science*, 326(5950):289–293, 2009.
- Suhas SP Rao, Miriam H Huntley, Neva C Durand, Elena K Stamenova, Ivan D Bochkov, James T Robinson, Adrian L Sanborn, Ido Machol, Arina D Omer, Eric S Lander, et al. A 3d map of the human genome at kilobase resolution reveals principles of chromatin looping. *Cell*, 159(7):1665–1680, 2014.
- Suhas SP Rao, Su-Chen Huang, Brian Glenn St Hilaire, Jesse M Engreitz, Elizabeth M Perez, Kyong-Rim Kieffer-Kwon, Adrian L Sanborn, Sarah E Johnstone, Gavin D Bascom, Ivan D Bochkov, et al. Cohesin loss eliminates all loop domains. *Cell*, 171(2):305–320, 2017.
- Herbert Edelsbrunner, David Letscher, and Afra Zomorodian. Topological persistence and simplification. In *Proceedings 41st annual symposium on foundations of computer science*, pages 454–463. IEEE, 2000.
- David Cohen-Steiner, Herbert Edelsbrunner, and Dmitriy Morozov. Vines and vineyards by updating persistence in linear time. In *Proceedings of the twenty-second annual symposium on Computational geometry*, pages 119–126, 2006.
- Chao Chen and Michael Kerber. Persistent homology computation with a twist. In *Proceedings 27th European Workshop on Computational Geometry*, volume 11, pages 197–200, 2011.
- Jesse R Dixon, Siddarth Selvaraj, Feng Yue, Audrey Kim, Yan Li, Yin Shen, Ming Hu, Jun S Liu, and Bing Ren. Topological domains in mammalian genomes identified by analysis of chromatin interactions. *Nature*, 485(7398):376–380, 2012.
- Tamal K Dey, Dayu Shi, and Yusu Wang. Simba: An efficient tool for approximating rips-filtration persistence via simplicial batch collapse. *Journal of Experimental Algorithmics (JEA)*, 24:1–16, 2019.
- Anirudh Som, Hongjun Choi, Karthikeyan Natesan Ramamurthy, Matthew P Buman, and Pavan Turaga. Pi-net: A deep learning approach to extract topological persistence images. In *Proceedings of the IEEE/CVF Conference on Computer Vision and Pattern Recognition Workshops*, pages 834–835, 2020.